Small-molecule CBP/p300 histone acetyltransferase inhibition mobilizes leukocytes from the bone marrow via the endocrine stress response

Jaschke, Nikolai P.; Breining, Dorit; Hofmann, Maura; Pählig, Sophie; Baschant, Ulrike; Oertel, Reinhard; Traikov, Sofia; Grinenko, Tatyana; Saettini, Francesco; Biondi, Andrea; Stylianou, Myrto; Bringmann, Henrik; Zhang, Cuiling; Yoshida, Tomomi M. [**and 9 more**]

How to cite

JASCHKE, Nikolai P. et al. Small-molecule CBP/p300 histone acetyltransferase inhibition mobilizes leukocytes from the bone marrow via the endocrine stress response. In: Immunity, 2024, vol. 57, n° 2, p. 364–378.e9. doi: 10.1016/j.immuni.2024.01.005

This publication URL: https://archive-ouverte.unige.ch/unige:177759

Publication DOI: 10.1016/j.immuni.2024.01.005

CellPress
OPEN ACCESS

Immunity

Article

Small-molecule CBP/p300 histone acetyltransferase inhibition mobilizes leukocytes from the bone marrow via the endocrine stress response

Nikolai P. Jaschke,[1,2,17,*] Dorit Breining,[1,15] Maura Hofmann,[1,15] Sophie Pählig,[1] Ulrike Baschant,[1] Reinhard Oertel,[3] Sofia Traikov,[4] Tatyana Grinenko,[5,6] Francesco Saettini,[7] Andrea Biondi,[8,9,10] Myrto Stylianou,[11] Henrik Bringmann,[11] Cuiling Zhang,[2] Tomomi M. Yoshida,[2] Heike Weidner,[1] Wolfram C. Poller,[12] Filip K. Swirski,[12] Andy Göbel,[1] Lorenz C. Hofbauer,[1] Martina Rauner,[1] Christoph Scheiermann,[13,14,16] Andrew Wang,[2,16] and Tilman D. Rachner[1,16]

[1]Division of Endocrinology, Department of Medicine III, Faculty of Medicine, Technische Universität Dresden, Dresden, Germany
[2]Department of Internal Medicine (Rheumatology, Allergy & Immunology) and Department of Immunobiology, Yale School of Medicine, New Haven, CT, USA
[3]Institute of Clinical Pharmacology, Faculty of Medicine, Technische Universität Dresden, Dresden, Germany
[4]Max-Planck Institute of Molecular Cell Biology, Dresden, Germany
[5]Institute of Clinical Chemistry and Laboratory Medicine, Faculty of Medicine, Technische Universität Dresden, Dresden, Germany
[6]Shanghai Institute of Hematology, State Key Laboratory of Medical Genomics, National Research Center for Translational Medicine at Shanghai, Ruijin Hospital Affiliated to Jiao Tong University School of Medicine, Shanghai, China
[7]Tettamanti Research Center, University of Milano-Bicocca, University of Milano Bicocca, Monza, Italy
[8]Centro Tettamanti, Fondazione IRCCS San Gerardo dei Tintori, Monza, Italy
[9]Pediatria, Fondazione IRCCS San Gerardo dei Tintori, Monza, Italy
[10]Dipartimento di Medicina e Chirurgia, Università degli Studi Milano-Bicocca, Monza, Italy
[11]Biotechnology Center (Biotec) Technische Universität Dresden, Dresden, Germany
[12]Cardiovascular Research Institute, Icahn School of Medicine at Mount Sinai, New York, NY, USA
[13]Department of Pathology and Immunology, Faculty of Medicine, University of Geneva, Geneva, Switzerland
[14]Biomedical Center (BMC), Institute for Cardiovascular Physiology and Pathophysiology, Walter Brendel-Center for Experimental Medicine (WBex), Faculty of Medicine, Ludwig-Maximilians-Universität Munich, Planegg-Martinsried, Germany
[15]These authors contributed equally
[16]These authors contributed equally
[17]Lead contact
*Correspondence: nikolai.jaschke@yale.edu
https://doi.org/10.1016/j.immuni.2024.01.005

SUMMARY

Mutations of the CBP/p300 histone acetyltransferase (HAT) domain can be linked to leukemic transformation in humans, suggestive of a checkpoint of leukocyte compartment sizes. Here, we examined the impact of reversible inhibition of this domain by the small-molecule A485. We found that A485 triggered acute and transient mobilization of leukocytes from the bone marrow into the blood. Leukocyte mobilization by A485 was equally potent as, but mechanistically distinct from, granulocyte colony-stimulating factor (G-CSF), which allowed for additive neutrophil mobilization when both compounds were combined. These effects were maintained in models of leukopenia and conferred augmented host defenses. Mechanistically, activation of the hypothalamus-pituitary-adrenal gland (HPA) axis by A485 relayed shifts in leukocyte distribution through corticotropin-releasing hormone receptor 1 (CRHR1) and adrenocorticotropic hormone (ACTH), but independently of glucocorticoids. Our findings identify a strategy for rapid expansion of the blood leukocyte compartment via a neuroendocrine loop, with implications for the treatment of human pathologies.

INTRODUCTION

The bone marrow is the central reservoir for leukocytes, which include specialized populations such as neutrophils, monocytes, and B lymphocytes. These cells arise from hematopoietic precursors and are released into the blood stream to reach distant tissue compartments.[1] Leukocyte compartment sizes in the blood and tissues fluctuate physiologically within dynamic ranges.[2–4] As a function of demand, as occurs in response to infections, injury, or stress, compartment sizes of leukocytes are modulated for host defense and returned to homeostasis when the demand is no longer present.[5,6] Leukocyte numbers and their distribution are controlled at the level of production, mobilization from organ reservoirs, trafficking cues directing cells to sites of demand as well as their rate of local degradation.[7] A variety of cell-autonomous

and non-cell-autonomous mechanisms that program these control mechanisms exist.[3,8–11]

Bone marrow function and leukocyte trafficking are subject to top-down control by the central nervous system (CNS), which integrates peripheral inputs to generate adaptive leukocyte responses.[12] These responses are mediated by different effectors including neuro-humoral circuits involving the hypothalamus-pituitary-adrenal gland (HPA) axis and the sympathetic nervous system (SNS).[7,10,13,14] Re-programming of leukocyte compartmentalization has trade-offs given the homeostatic roles that leukocytes play, and less well-studied programs return leukocyte compartments to homeostatic set-points once host insults have been resolved.[15–17] Conversely, loss of homeostatic control of leukocyte compartmentalization can be detrimental as exemplified by pathologic conditions, where normal "checkpoints" are dysregulated. This may lead to cases in which circulating leukocyte counts in the blood stream are barely detectable (e.g., acquired or genetic bone marrow failure) or excessively elevated as seen in patients with acute leukemia.

Despite increasing knowledge of how leukocyte compartments are controlled, pharmacological interventions to interfere with the production, degradation, and localization of leukocytes to correct hematologic pathologies, diseases of acute and chronic inflammation, or augment adaptive host defenses remain relatively limited. Available approaches include granulocyte colony-stimulating factor (G-CSF) derivatives, CXC-motif chemokine receptor 4 (CXCR4) antagonists (e.g., plerixafor/AMD3100), or inhibitors of the integrin very late antigen 4 (VLA4).[18,19] In the clinics, G-CSF derivatives remain the treatment of choice for neutropenia, whereas VLA4 or CXCR4 inhibitors are not approved for this indication. Although the prophylactic use of G-CSF effectively reduces the incidence and severity of neutropenia in chemotherapy-exposed individuals, G-CSF supplementation does not confer clear benefits in the setting of acute neutropenic fever.[19–22] G-CSF derivatives are generally well tolerated, but they can come with adverse events, which vary in frequency and severity.[19] As such, the pharmacological interference with leukocyte and particularly neutrophil compartmentalization is an underexplored space with an urgent need for innovation.

Extreme deviations from physiology as found in rare genetic diseases can be instructive to identify novel and druggable therapeutic targets.[23] Severe congenital neutropenia (SCN) is an illustrative case study since affected individuals display the two extreme ends of bone marrow phenotypes across their lifetime: loss of function (congenital neutropenia) to gain of function (acute myeloid leukemia).[24] The leukemic transformation of the disease is characterized by the acquisition of a distinct mutational landscape, which is not present during the cytopenic phase.[25] This landscape includes mutations in *RUNX1, SUZ12, ASXL1,* and *CSF3R* (missense mutation) as well as E1A-associated protein p300 (*EP300*, also referred to as "p300"), among others. We considered EP300 as a potential therapeutic target because loss of function of p300 in animal models is sufficient to both impair hematopoiesis (when deleted prenatally) and induce leukocytosis or leukemia in later life.[26,27] EP300 and its ortholog cyclic-adenosine-monophosphate-response-element-binding protein (CREBBP, also known as "CBP") share 90% sequence homology and are built from 8 functionally distinct domains, one of which confers histone acetyltransferase (HAT) activity.[28] The mutation in patients with SCN linked to leukemic transformation is located within the HAT-domain-encoding genetic sequence (c5030_5036delTGGAGAC),[25] suggestive of functional relevance to leukocyte homeostasis. These observations raise the question whether the HAT domain of CBP/p300 can be targeted pharmacologically to modulate leukocyte compartment sizes ("leukocytosis on demand"). Here, we demonstrate that competitive, reversible, small-molecule-mediated inhibition of the CBP/p300 HAT domain triggers acute and transient leukocyte mobilization from the bone marrow, which is relayed by a neuroendocrine loop of the HPA axis.

RESULTS

CBP/p300 HAT inhibition triggers transient leukocytosis

We used the spirocyclic, small-molecule CBP/p300 HAT inhibitor A485, which reversibly competes with acetyl coenzyme A (CoA) for binding to the HAT domain's catalytic center and exhibits high selectivity for CBP and p300 compared with other HATs (Figures S1A and S1B).[29] The crystal structure of the HAT-binding pocket in complex with A485 has previously been published.[29] We predicted that this mechanism of action should result in a rapid increase in cellular acetyl CoA levels and confirmed this hypothesis in primary murine cells (bone marrow-derived macrophages) (Figure S1C).

Wild-type (WT) mice injected intraperitoneally (i.p.) with A485 developed substantial leukocytosis within 2 h compared with vehicle-treated controls (Figure 1A), which resulted from increased numbers of most leukocyte populations in the blood, including neutrophils, B lymphocytes, and monocytes, whereas T lymphocytes, red blood cell, and platelet counts remained unchanged (Figures 1B, 1C, S1D, and S1E). Moreover, hematopoietic stem and progenitor cells ($Lin^{-}Sca1^{+}cKit^{+}Cd150^{+}CD48^{-}$) were rare in the circulation, irrespective of vehicle or A485-exposure (Figure S1F), suggesting that the leukocyte response induced by A485 was specific. The efficacy of the compound to expand blood leukocytes was validated in a second animal facility, both sexes and independent of handlers (Figures 1 and S1G–S1I). Leukocytosis occurred in a dose-dependent fashion with a ceiling effect, was not subject to relevant tachyphylaxis, and could be recapitulated with an independent, non-spirocyclic CBP/p300 HAT inhibitor (C646)[30] (Figures 1D and S1J–S1L). By contrast, inhibition of the protein's bromodomain[31]—which confers DNA binding—or the HAT domain of another major mammalian HAT (Tip60) did not induce leukocytosis (Figures S1M and S1N).

To understand the pharmacokinetics of A485, we profiled the distribution of the drug in the circulation and across different tissues using liquid chromatography-tandem mass spectrometry (LC-MS/MS). We found that the serum concentration of A485 peaked rapidly following i.p. injection and dropped to barely detectable limits by 12 h and non-detectable amounts by 24 h (Figure S2A). We noted accumulation of A485 in most tissues analyzed including the bone marrow, adipose tissue (AT), liver, spleen, aorta, and the kidney (Figure S2B). In line with previous reports,[29] we failed to detect relevant levels in whole

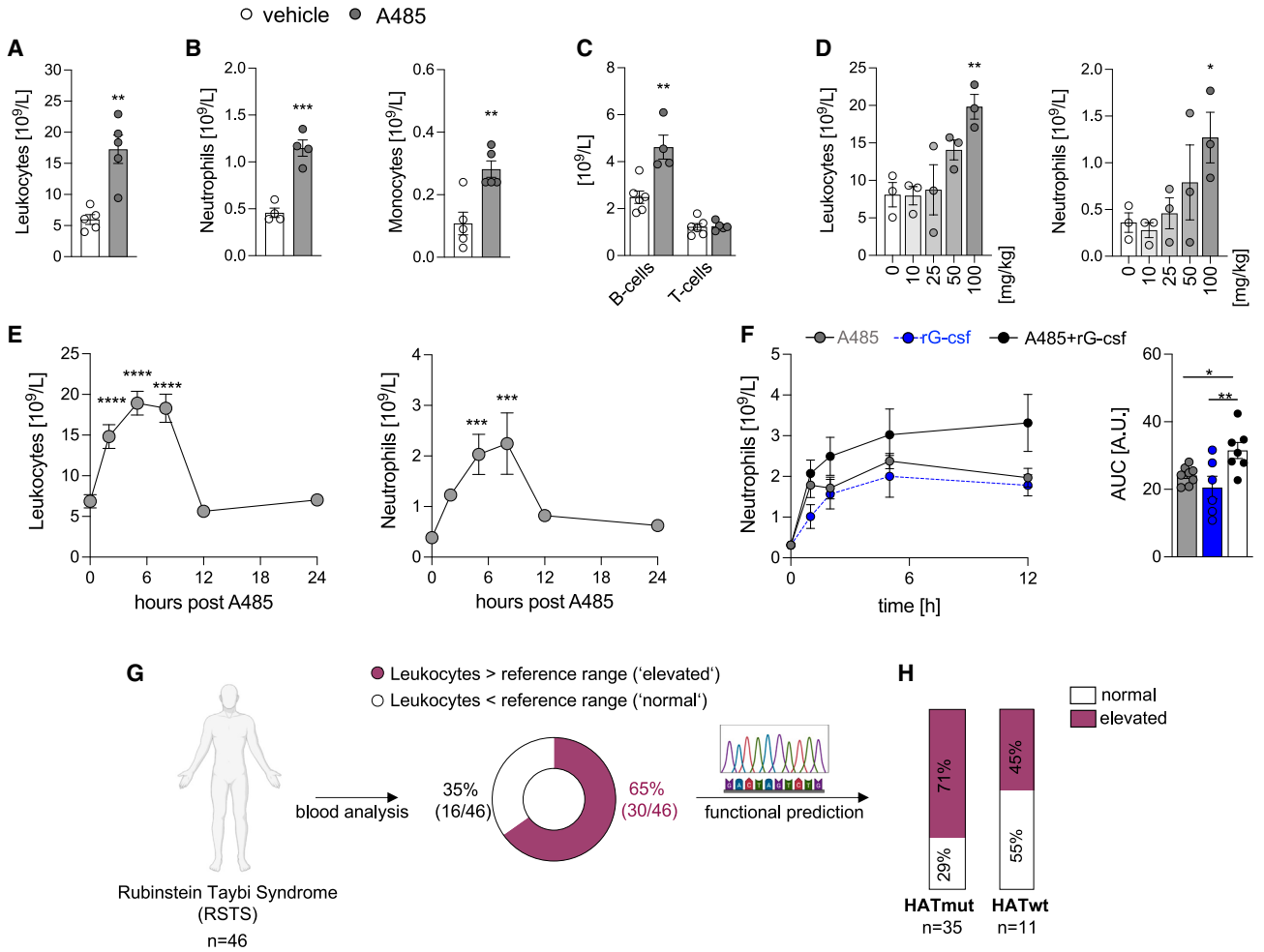

Figure 1. CBP/p300 HAT inhibition triggers transient leukocytosis

(A) Blood leukocytes in C57BL/6J wild-type (WT) mice 2 h following A485 (100 mg/kg) or vehicle injection (n = 4–5/group).

(B and C) Neutrophil, monocyte, and B and T lymphocyte counts in the same mice assessed by flow cytometry.

(D) Blood leukocytes and neutrophils in response to increasing concentrations of A485 or vehicle solution ("0") (n = 3/group).

(E) Dynamic changes in blood leukocyte and neutrophil numbers at different time points following A485 injection (n = 5–9/time point).

(F) Neutrophil kinetics in the blood over time in response to treatment with recombinant murine G-CSF i.v., A485 i.p., or the combination of the two drugs (n = 6–8/group). Quantification of the neutrophil area under the curve (AUC) (0–12 h) from the same animals is shown on the right.

(G) Schematic illustration of the percentage of individuals in a cohort of patients with Rubinstein-Taybi syndrome (RSTS) exhibiting leukocyte counts above (elevated) or below ("normal") the age-adjusted upper reference limit of normal (n = 46 total).

(H) Percentage of patients with or without elevated leukocyte counts as stratified by mutational profile (HAT domain likely functionally affected: HATmut or not affected: HATwt). Data are shown as mean ± SEM or frequency of total *p < 0.05, **p < 0.01, ***p < 0.001, ****p < 0.0001.

(A–C) Unpaired, two-tailed Student's t test (D–F) one-way ANOVA with Holm Sidak's post hoc test.

brain lysates, arguing against blood-brain barrier penetration (Figure S2B).

The dynamics of leukocytes in the blood closely paralleled these kinetics: their numbers started to rise within 1 h upon A485 exposure, peaked between 4 and 6 h, and returned to baseline by 12 h post-injection (Figures 1E, S2C, and S2D). This pattern was identical for neutrophils, lymphocytes, and monocytes (Figures 1E and S2D). One week after a single bolus of A485, leukocyte counts were indistinguishable from controls, arguing against a lasting effect on these cells (Figure S2E). We found no evidence for toxicity as mice appeared and behaved normal, did not lose weight, and markers of organ damage were similar between groups (Figures S2F and S2G). We also did not detect signs of toxicity in murine bone-marrow-derived macrophages *in vitro* (Figure S2H).

We next compared the efficacy of A485 to expand blood leukocytes with established pharmaceuticals and first focused on G-CSF, a potent endogenous regulator of neutrophil compartments and the treatment of choice for neutropenia in humans.[32] We injected recombinant murine G-CSF (rG-CSF, 250 μg/kg as previously reported[33]) i.v. or i.p. in mice and compared the resulting neutrophil kinetics with A485. We found that dynamic changes in circulating neutrophils were comparable between A485 and G-CSF, irrespective of the route of administration,

although neutrophilia onset appeared slightly faster with A485 (Figures 1F, S3A, and S3B). Importantly, the combination of the two drugs resulted in superior neutrophil mobilization compared with treatment with either agent alone (Figure 1F). We further noted that, after 24 h, leukocytes, neutrophils, and monocytes were substantially more abundant in the circulation of G-CSF-, compared with A485-treated mice (Figure S3C), suggesting that the A485 neutrophil response is shorter and distinct from G-CSF. Inhibition of CXCR4 is another clinically used approach to mobilize leukocytes and hematopoietic stem cells.[34] We observed that acute neutrophil and leukocyte kinetics were similar between the CXCR4 antagonist AMD3100 and A485 (Figure S3D).

To study potential analogies between our observations in mice and human biology, we obtained data from a previously characterized cohort of patients with Rubinstein-Taybi syndrome (RSTS), a rare developmental disorder with an estimated prevalence of 1:125,000 among live-born infants. RSTS is characterized by a distinct phenotype, which includes a short stature, learning difficulties, and facial features. The inheritance of the disease follows an autosomal dominant pattern.[35] Heterozygous mutations in *CREBBP* (CBP) cause RSTS type 1, while those in *EP300* (p300) result in RSTS type 2. The two types of RSTS account for 55% and 8% of cases, respectively.[36] We included 46 individuals (21 females and 25 males) of whom full genetic data and leukocyte counts were available (Figure 1G). The median age of patients at diagnosis was 11 years (range: 1–43 years). Consistent with the literature, RSTS type 1 was much more common than RSTS type 2 in our cohort (40 vs. 6 cases). The majority individuals (65%) displayed leukocyte counts above the age-adjusted upper limit of normal (“elevated”) (Figure 1G). We calculated that this distribution was skewed compared with expected frequencies in the general population[37,38] ($p < 0.0001$, χ^2 test, two-tailed). Patients were then stratified according to their mutational profile: the first group comprised mutations that were predicted to involve the HAT domain (missense within/frameshift before or within/deletion before or including the HAT domain) of *CREBBP* or *EP300* (n = 35), while the second group included all other mutations (n = 11) (Figure 1H). HAT-domain-affecting mutations (referred to as “HATmut”) were linked to leukocytosis in 71% (25/35) of cases, while those that spared it (“HATwt”) were less likely associated with this phenotype (45%) ($p = 0.11$, χ^2 test, two-tailed) (Figure 1H). The absolute number of leukocytes did not differ between the two groups (Figure S3E). Altogether, these data support a function of the CBP/p300 HAT domain in controlling leukocyte compartment sizes in mice and humans.

A485-induced leukocytosis augments host defenses

We then aimed to explore the therapeutic utility of our findings and first used Vav1-Nup98-Hoxd13 mice, an experimental model of myelodysplastic syndrome (referred to as “MDS”) (Figure 2A). We found that the expansion of the blood leukocyte compartment in response to A485 was maintained in MDS animals (Figure 2B). Because neutropenia is the clinically most relevant leukopenia, but neutrophils were only mildly reduced in these mice (Figure 2A), we next moved to a model of chemotherapy-associated bone marrow injury, which we induced by 5-fluorouracil (5FU) administration (Figure 2C). As expected, 5FU treatment resulted in significant leuko- and neutropenia, which could be acutely recovered by A485 treatment (Figure 2D). Accordingly, we investigated whether these effects would protect immunocompromised hosts against infections, which are major drivers of mortality in such individuals.[39,40] We modeled *Listeria monocytogenes* sepsis, where neutrophils are indispensable for host defense,[41] and introduced the pathogen in the context of overt 5FU-induced pancytopenia (day 6 post 5FU) (Figures 2E and 2F). To directly test the functional effects of A485-induced leukocyte mobilization, we did not administer antibiotics. A485 was injected in a therapeutic fashion after infection had been established (Figure 2E). Although we did not note mortality in mice without bone marrow injury during the observational period, leukopenic hosts treated with vehicle solution lost weight, became moribund, and succumbed to disease (Figures 2G and 2H). By contrast, a single bolus of A485 was sufficient to ameliorate disease trajectories as reflected by reduced weight loss and improved survival (Figures 2G and 2H). This protective effect was linked to enhanced pathogen clearance as indicated by diminished recovery of viable bacteria from liver tissue lysates of A485-treated animals (Figure 2I). Less pronounced changes were noted in the spleen (Figure 2J).

Taken together, our data imply a therapeutic potential of A485 for the acute recovery of leukocyte counts and augmentation of host defenses in the presence of bone marrow injury.

A485 mobilizes leukocytes from the bone marrow

Having established that A485 induced a functional leukocytosis, we next sought to understand its mechanism of action. First, we reasoned that a prolonged half-life could not explain leukocytosis due to its rapid onset. Second, we found no evidence for induction of “emergency hematopoiesis” as numbers of progenitor populations in the bone marrow were unchanged by A485 (Figure S4A). Third, blocking lymphocyte egress from lymph nodes by sphingosine-1-phosphate receptor antagonism also did not impair the ability of A485 to increase leukocyte and specifically, lymphocyte counts (Figure S4B). Therefore, we focused on bone marrow mobilization as a potential mechanism of A485-induced leukocytosis.

To test whether A485 mobilized cells from the bone marrow, we used a previously described cell tracking approach,[13] in which bone marrow cells from CD45.1 mice were adoptively transferred into CD45.2 mice by intravenous injection (Figure 3A). By 8 h post transplantation, transferred cells ($CD45.1^+$) had efficiently migrated from the blood into the bone marrow (Figures 3B and S4C) and could be mobilized from this compartment by A485: both CD45.1- and CD45.2-positive cells increased in the circulation and peripheral tissues following injection of the drug, while their numbers decreased significantly only in the bone marrow (Figures 3C and S4D). Consistent with previous reports,[13] we found that the relative drop in leukocytes in the bone marrow was modest (Figure 3C) but sufficient to explain the changes in the periphery due to the large number of cells stored in this compartment throughout the body. This was supported by estimate calculations based on our cell tracking data (Figure 3D) as well as published analyses of the numbers and distribution of leukocytes across tissues.[42]

Using fluorophore-conjugated antibodies, we found that the distribution of cells within tissues in response to A485 was

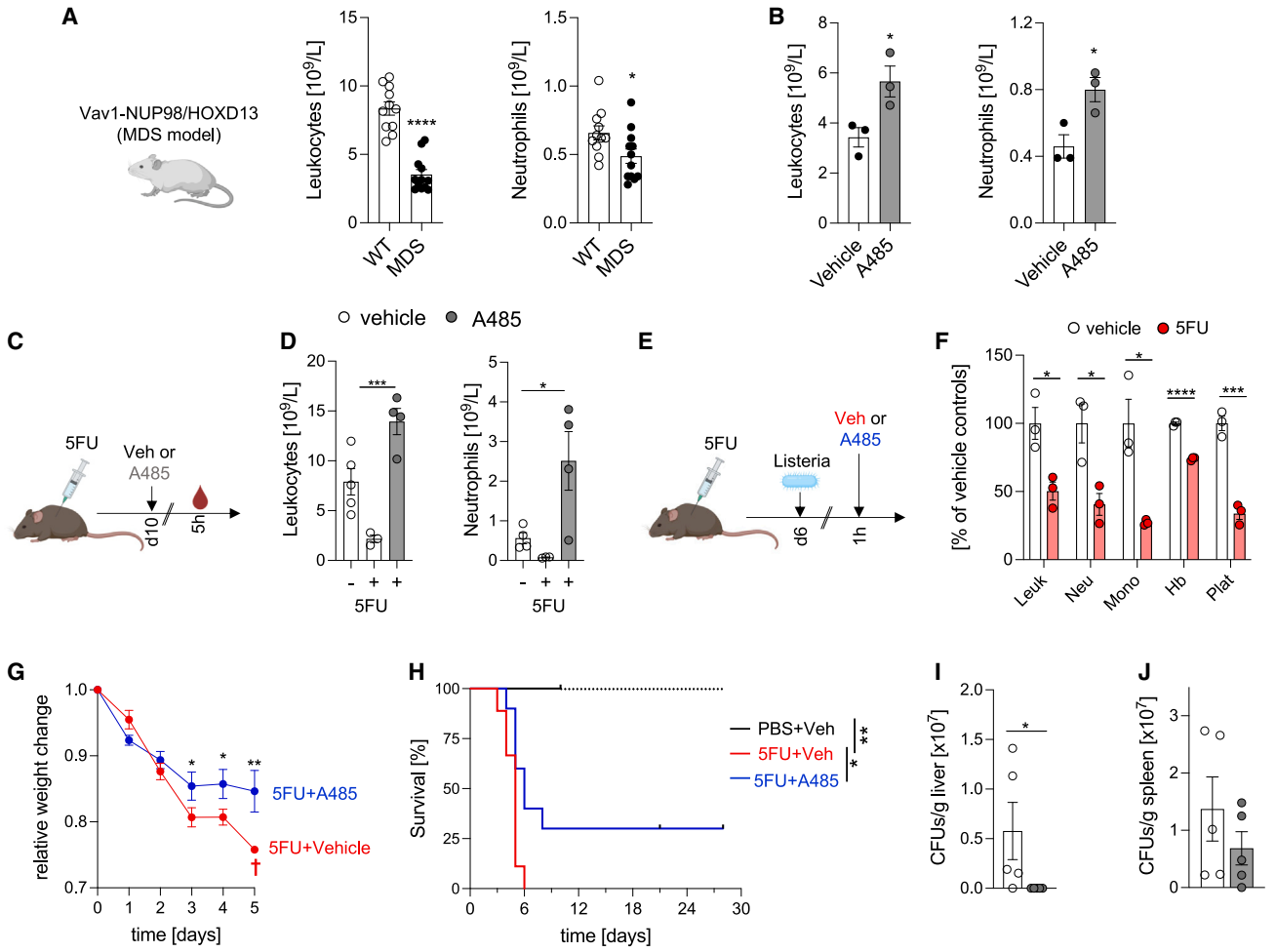

Figure 2. A485-induced leukocytosis augments host defenses

(A) Leukocyte and neutrophil blood counts in 12-week-old female Vav1-NUP98-HOXD13 mice, a model for myelodysplastic syndrome (MDS), or wild-type littermate controls (WT) (n = 11–12/group).

(B) Blood leukocyte and neutrophils in MDS mice 2 h following A485 or vehicle treatment (n = 3/group).

(C) Experimental design.

(D) Leukocyte and neutrophil counts in naive (PBS injected) or 5-flurouracil (5FU)-treated C57BL/6J WT mice exposed to vehicle solution (white) or A485 (gray) on day 10 of the experiment (refers to experimental design in (C) (n = 3–5/group). Blood was collected 5 h post-injection.

(E) Experimental design of the bone marrow injury and bacterial sepsis model.

(F) Blood analysis of mice on day 6 following 5FU (150 mg/kg) exposure. Results are expressed as percentage of vehicle controls (n = 3/group).

(G) Relative change in body weight from baseline in mice infected with 7.5 × 10^4 CFUs *Listeria monocytogenes* on day 6 after 5FU exposure, followed by treatment with a single bolus of A485 or vehicle 1 h post-infection. (n = 2–10/group; low sample size beyond day 3 due to mortality. Cross symbol indicates 100% mortality.)

(H) Survival curves. 5FU-treated mice were challenged with 7.5 × 10^4 CFUs, while PBS controls received 1 × 10^5 CFUs. The latter group was sacrificed on day 9 without any signs of sickness. The dashed line corresponds to predicted survival of immunocompetent (PBS-treated) mice (n = 9–10 for 5FU groups, n = 3 for PBS group).

(I and J) Number of colony-forming units (CFUs) of *Listeria monocytogenes* recovered from liver and spleen lysates on day 2 of the infection. Results were normalized according to tissue weight (n = 5/group). Data are shown as mean ± SEM. *p < 0.05, **p < 0.01, ***p < 0.001, ****p < 0.0001.

(A, B, and F) Unpaired, two-tailed Student's t test (D) one-way ANOVA with Holm Sidak's post hoc test. (G) Two-way ANOVA with Fisher's least square difference (LSD), (H) Mantel-Cox test, and (I) Mann-Whitney U test.

mostly intravascular, while some cells had also emigrated (Figures 3E, 3F, S4E, and S4F). Likewise, cells recruited from the bone marrow included those from intra- (B lymphocytes) and extravascular (neutrophils) pools (Figures 3G and S4G). Of note, A485 could no longer increase leukocyte counts in sub-lethally irradiated mice with acute hematopoietic failure (day 3 post irradiation), where bone marrow leukocytes were strongly diminished (Figure 3H).

In summary, these results indicate that small-molecule-mediated CBP/p300 HAT inhibition rapidly and transiently expands the blood leukocyte compartment primarily by mobilizing cells from the bone marrow. However, we cannot formally rule

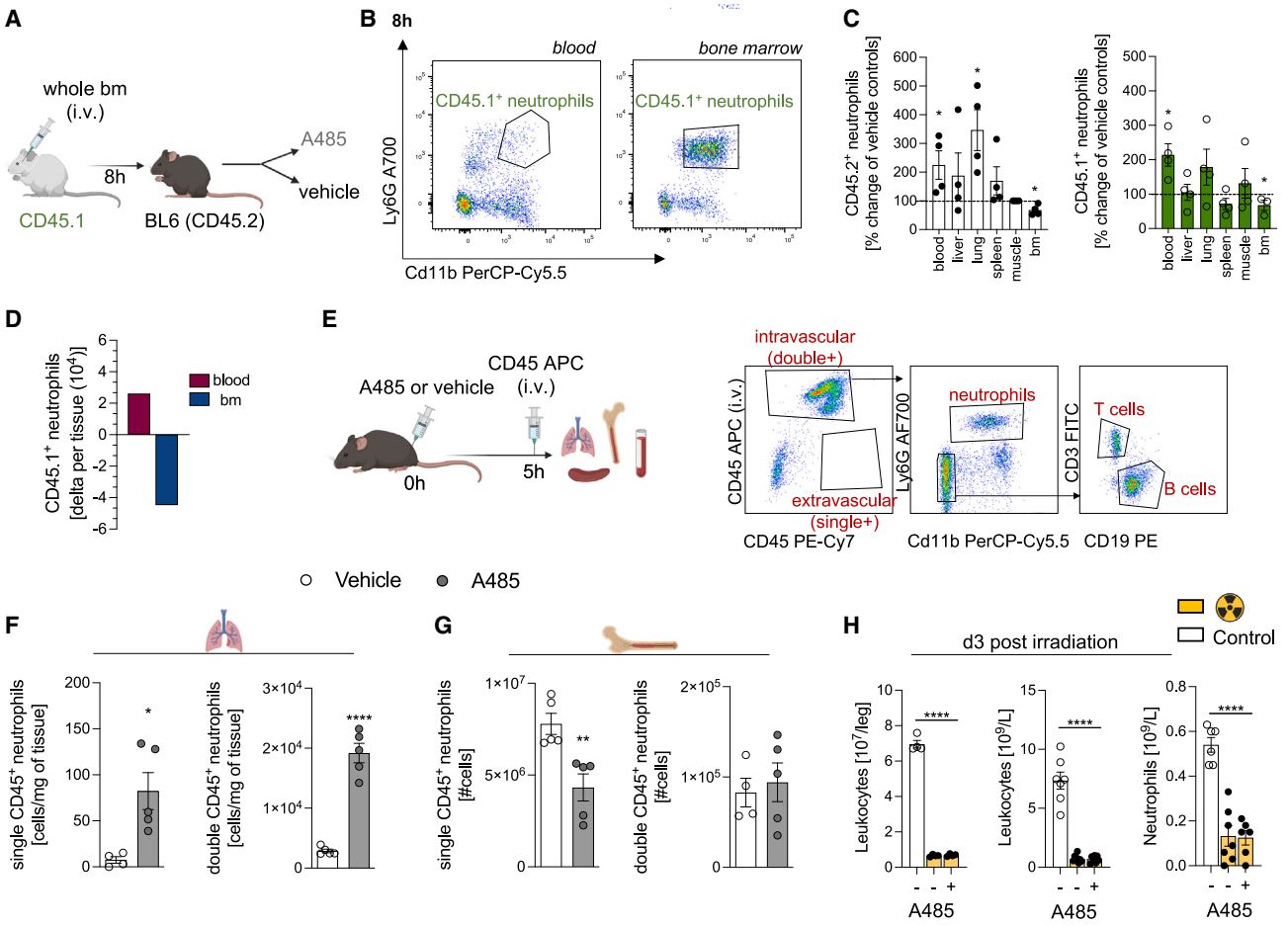

Figure 3. A485 mobilizes leukocytes from the bone marrow

(A) Experimental design.

(B) Exemplary flow cytometry plot of adoptively transferred CD45.1 neutrophils in the blood and bone marrow 8 h post i.v. injection of cells.

(C) Quantification of endogenous CD45.2 and transferred CD45.1 neutrophils in different organs 5 h after A485 injection expressed as percentage of the mean neutrophil number in the respective organ of vehicle-treated mice (n = 4/group).

(D) Estimated loss of transferred CD45.1 neutrophils in the bone marrow vs. gain in the blood.

(E) Experimental design of intravascular labeling of leukocytes using fluorophore conjugated anti-CD45 antibodies (left) with the corresponding gating strategy (right). Exemplary plots are shown.

(F) Extravascular (referred to as "single CD45$^+$") and intravascular ("double CD45$^+$") neutrophils in lung tissue 5 h after A485 or vehicle injection. Results were normalized according to tissue weight (n = 5/group).

(G) Intra- or extravascular neutrophils in the bone marrow of the same animals.

(H) Quantification of leukocytes in the bone marrow and leukocytes and neutrophils in the blood 3 days after sub-lethal irradiation followed by injection of A485 or vehicle (n = 3–4/group for bone marrow and n = 7/group for blood). Data are shown as mean ± SEM. *p < 0.05, **p < 0.01, ***p < 0.001, ****p < 0.0001.

(C, F, and G) Unpaired, two-tailed Student's t test (H) one-way ANOVA with Holm-Sidak's post hoc test.

out that demargination phenomena may also contribute to leukocytosis.

Distinct effector pathways drive changes in leukocyte subsets in response to A485

We then set out to explore the molecular mechanism underlying A485-induced bone marrow mobilization. The speed by which leukocytosis occurred in response to A485 led us to speculate that a tonic mechanism that retains cells in the bone marrow might be disrupted. CXCR4 signaling is induced by CXCL12 and regulates the cell surface expression of adhesion molecules, including VLA4, the latter of which is built from CD49d (encoded by *Itga4* in mice) and CD29 (*Itgb1*).[43,44] When CXCL12 levels decline, Cd49d is downregulated.[45] Peak leukocytosis in response to A485 was paralleled by reduced CD49d cell surface expression on B lymphocytes and neutrophils together with a concomitant decrease of the VLA4-binding partner vascular cell adhesion molecule 1 (VCAM1) on bone marrow endothelial cells as assessed by flow cytometry (Figures 4A and S5A). We further detected reduced CXCL12 protein levels in the circulation and bone marrow of A485-treated mice (Figures S5B and S5C). To understand which of these changes occurred first, we sampled mice 1 h post-injection, a time point prior to the onset of apparent leukocytosis. Here, HAT activity was already

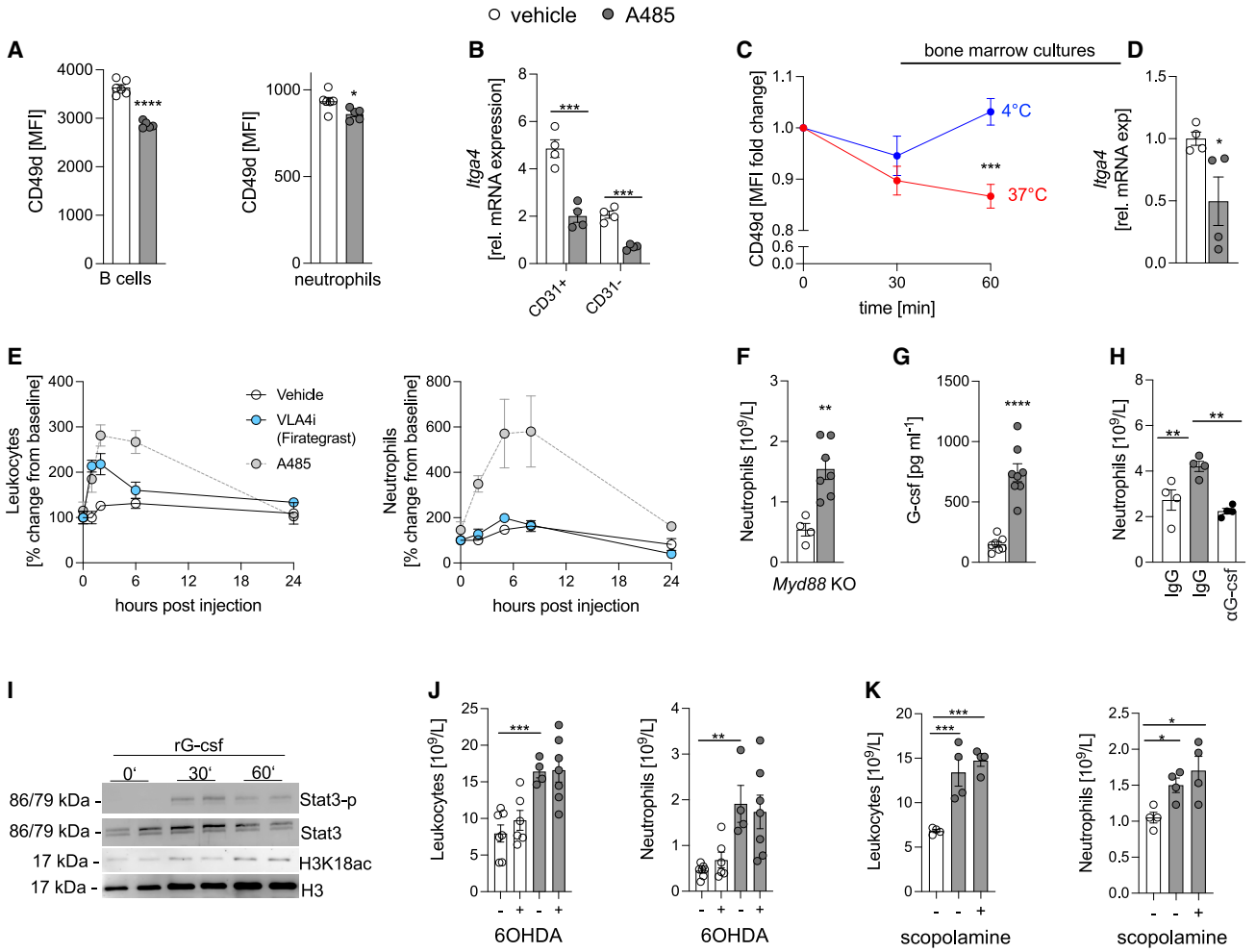

Figure 4. Distinct effector pathways drive changes in leukocyte subsets in response to A485

(A) Cell surface expression of the VLA44 subunit CD49d on B lymphocytes and neutrophils assessed by flow cytometry 5 h following A485 or vehicle injection (n = 5–6/group).

(B) Quantification of *Itga4* (encoding for Cd49d) mRNA levels in CD31$^+$ and CD31$^-$ bone marrow cells 1 h following A485 or vehicle injection assessed by qPCR (n = 4/group).

(C) Cell surface expression of Cd49d on CD45$^+$ cells in bone marrow cultures following exposure to 5 μM A485 for 30 or 60 min at 37 or 4°C *ex vivo*. Results are expressed as fold change compared with vehicle-treated controls (n = 3/time point).

(D) *Itga4* mRNA levels in bone marrow cultures treated with vehicle or A485 (5 μM) for 30 min assessed by qPCR.

(E) Dynamic changes in blood leukocytes and neutrophils upon VLA4 inhibition (by firategrast) or vehicle treatment expressed as percentage of the mean cell count at baseline (n = 4/group). A485 is overlayed for reference in light gray.

(F) Blood neutrophils in mice with global genetic Myd88 deletion (Myd88 KO) following vehicle or A485 administration. Blood was collected at 2 h post-injection (n = 4–7/group).

(G) Circulating G-CSF levels in vehicle and A485-treated mice 12 h post exposure to the respective substance (n = 8/group).

(H) Peak blood neutrophil levels (5 h post injection) in A485- or vehicle-exposed mice following pre-treatment with an anti-G-CSF antibody or isotype control (IgG) (n = 4/group).

(I) Immunoblot of acetylated lysine 18 of histone H3 (H3K18ac) in bone marrow cultures treated with recombinant murine G-CSF (rG-CSF) *ex vivo*. Stat3 phosphorylation was used as a positive control for confirmation of successful induction of CSF3R signaling.

(J) Blood leukocytes and neutrophils in A485- or vehicle-treated mice following chemical sympathectomy by 6-OHDA (+) or vehicle (PBS) injection (–) (n = 4–7/group). Blood was collected 5 h after drug exposure.

(K) Leukocytes and neutrophils in the blood 2 h following A485 or vehicle treatment with (+) or without (–) concomitant muscarinic receptor blockade by scopolamine (n = 4/group). Data are shown mean ± SEM. *p < 0.05, **p < 0.01, ***p < 0.001, ****p < 0.0001.

(A, B, D, F, and G) Unpaired, two-tailed Student's t test.

(C) Two-way ANOVA with Holm-Sidak's post hoc test.

(H, J, and K) One-way ANOVA with Holm-Sidak's post hoc test.

strongly suppressed as shown by reduced protein levels of acetylated lysine 18 residues of histone H3 (H3K18ac) in bone marrow cell lysates of A485-treated mice (Figure S5D). Isolation of $CD31^+$ and $CD31^-$ bone marrow cells demonstrated that *Cxcl12* transcript levels were indifferent between groups at this early time point, and Cxcl12 protein abundance was likewise unchanged (Figures S5E and S5F). By contrast, *Cxcr4* and *Itga4* expression was reduced in both $CD31^-$ and $CD31^+$ cells (Figures 4B and S5G). Using *ex vivo* cultures, we found that the downregulation of VLA4 involved transcriptional repression as well as internalization events, confirming a direct effect of A485 on the bone marrow (Figures 4C and 4D). We did not note changes in Cxcl12 protein secretion in the same system (Figure S5H), indicating that A485 modulates the niche via direct and indirect pathways. Pharmacological inhibition of VLA4 (VLA4i) by firategrast resembled A485-induced leuko- and lymphocytosis, but with lower amplitude and different dynamics, while eliciting much milder neutrophilia (Figures 4E and S5I). We further found that A485 did not inhibit leukocyte migration toward CXCL12 *in vitro* (Figure S5J), suggesting that the compound does not act as a CXCR4 antagonist upstream of VLA4. Together, these results indicate that, while lymphocytosis may result from disruption of VLA4-VCAM1-interactions, neutrophilia could not be explained by this mechanism. This led us to study other candidate pathways that may drive this response.

Neutrophil mobilization typically involves cytokine signaling.[5,46] However, inflammatory cytokines linked to emergency myelopoiesis and neutrophilia (tumor necrosis factor alpha, interleukin [IL]-1 beta) remained undetectable in the circulation of both A485 and vehicle-treated mice (Figures S6A and S6B). Consistently, disruption of IL-1-/Toll-like receptor family signaling by global genetic *Myd88* deletion did not interfere with A485-induced neutrophilia or leukocytosis (Figures 4F and S6C). We also found no evidence for type 1 interferon, alarmin, or IL-6 dependency of the drug's effects on leukocytes (Figures S6D–S6F).

Therefore, we next explored contributions of G-CSF signaling. We first measured the concentration of G-CSF in the circulation and detected increased levels in response to A485 treatment (Figure 4G). Administration of anti-G-CSF-antibodies diminished A485-induced neutrophilia while leaving total leukocyte and lymphocyte counts unchanged (Figures 4H and S6G). The lack of effect of G-CSF neutralization on lymphocytes was expected as these cells are not mobilized by G-CSF.[47] We did not detect changes in H3K18ac protein levels in bone marrow cultures treated with G-CSF, ruling out that CBP/p300 HAT activity resides downstream of the G-CSF receptor (CSF3R) (Figure 4I). We thus asked whether A485 and G-CSF converge onto a common effector cascade. We chose to manipulate the SNS as well as cholinergic signaling, both of which are required for G-CSF-induced bone marrow mobilization.[7,10] SNS outflow was dispensable for A485-triggered leukocytosis as chemical sympathectomy using 6-hydroxydopamine (6-OHDA) left neutrophilia, leuko-, and lymphocytosis intact (Figures 4J and S6H). These results were recapitulated in adrenoceptor beta 1/2 double-deficient mice (*Adrb1/b2* KO) (Figure S6I), which lack the receptor repertoire engaged by the SNS to modulate leukocyte compartments.[48] Likewise, the blood-brain barrier penetrating muscarinic receptor antagonist scopolamine did not interfere with neutrophilia or leukocytosis in response to A485 (Figure 4K). Lastly, combining A485 and G-CSF did not result in meaningful increases in total (sum of endo- and exogenous) G-CSF levels (Figure S6J), suggesting that the additive effects of the two compounds on neutrophils that we observed (Figure 1F) cannot be explained by augmented G-CSF activity. We conclude that A485 requires both G-CSF-dependent and -independent pathways to elicit neutrophilia.

The HPA axis is activated by A485

Our findings led us to hypothesize that the A485 leukocyte response was fueled by neurohumoral pathways. Therapeutic doses of glucocorticoids (GCs) trigger rapid-onset leukocytosis in humans, and GCs control leukocyte trafficking under homeostatic and stressful conditions.[49,50] Circulating levels of corticosterone (referred to as CORT)—the main endogenous GC in mice—were strongly increased in response to A485 (Figure 5A), indicative of HPA-axis activation.

The HPA axis operates according to control loop principles[51] and is built from 3 main components (Figure 5B). Unlike forskolin—which promotes cyclic adenosine monophosphate (cAMP) production[52]—increasing concentrations of A485 had no effect on the transcription of key steroidogenic enzymes and CORT release of adrenal cortical cells (Y1) *in vitro* (Figures 5C and S7A), arguing against a direct effect of the drug on the adrenal gland. We thus asked whether A485 induces HPA-axis activity at the level of the CNS. Consistent with this idea, the mRNA abundance of *cFos*—an immediate-early gene indicative of neuronal activity—was nearly twice as high in hypothalamus cell lysates of A485-treated animals compared with controls 1 h post-injection (Figure 5D). We further observed that cFos protein was elevated in the paraventricular nucleus (PVN) of the hypothalamus, where corticotropin-releasing hormone (CRH)-producing neurons reside (Figure 5E). These changes translated into augmented systemic adrenocorticotropic hormone (ACTH) release (Figure 5F). We thus screened several mechanisms by which A485 may engage the HPA axis at the level of the hypothalamus.

Some hypothalamic neuronal populations are surrounded by permeable capillary networks, which allow for exposure to systemic cues.[53] However, we found that levels of A485 in the hypothalamus were as low as in other parts of the brain, and hypothalamic explants did not upregulate *cFos* when exposed to the drug *ex vivo* (Figures 5G and S7B), suggesting that A485 acts on the PVN via an indirect route. Systemic hypoglycemia was not the underlying trigger as blood glucose levels increased, rather than decreased upon A485 treatment (Figure 5H). Body temperature declined in response to A485 exposure, but warmth supplementation did not prevent CORT release, demonstrating that core body temperature is not correlated with HPA-axis activation (Figures 5I and 5J). We also found no evidence for contributions of IL-6 signaling (Figure S7C), which is physiologically induced in response to stress and regulates the HPA axis.[54,55] We further noted that HPA-axis activation did not require nociception or consciousness because mice subjected to ablation of $TRPV1^+$ sensory neurons using resiniferatoxin (RTX) or ketamine/xylazine (ket/xyl) anesthesia still showed strongly elevated levels of CORT and leukocytes in response to the drug (Figures 5K, 5L, S7D, and S7E). We thus wondered whether sensory nerve fibers that are spared by RTX (i.e., $TRPV1^-$) may

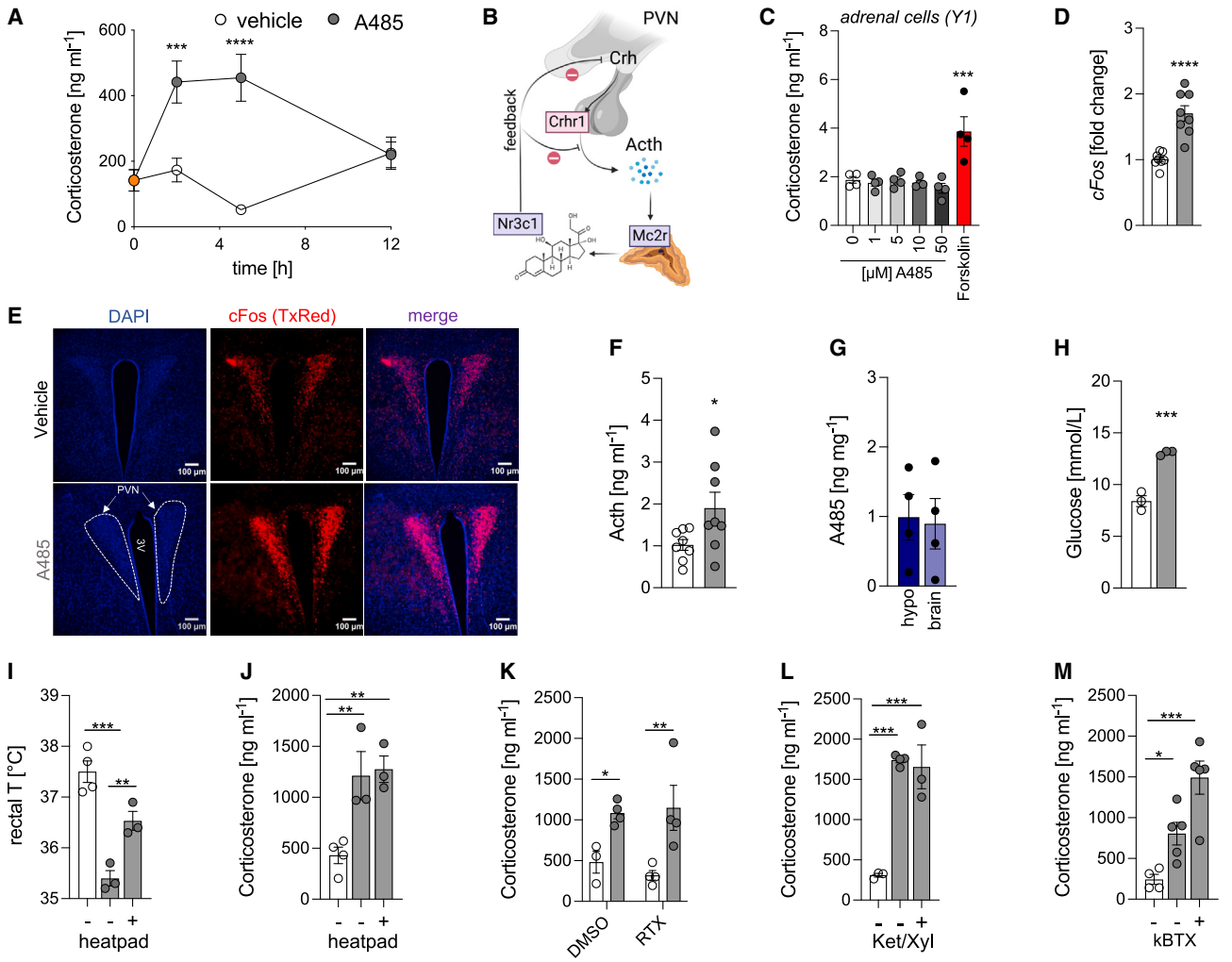

Figure 5. The HPA axis is activated by A485

(A) Circulating CORT levels over time assessed by ELISA in response to vehicle or A485 treatment. Baseline levels were determined in 4 randomly sampled mice (orange dot) prior to drug injection (n = 3–6/time point).

(B) Design of the HPA-axis. Neurons of the paraventricular nucleus (PVN) secrete corticotropin-releasing hormone (CRH) into the hypophyseal portal system, which triggers adrenocorticotropic hormone (ACTH) release from the anterior pituitary via CRH receptor 1 (CRHR1). ACTH promotes glucocorticoid (GC) secretion from the adrenal cortex through melanocortin receptor 2 (Mc2r). GCs bind to the glucocorticoid receptor (Nr3c1) and exert negative feedback on HPA-axis activity.

(C) CORT concentration in cell culture supernatants of adrenal cortical Y1 cells exposed to vehicle (DMSO), increasing concentrations of A485 or the cAMP inductor forskolin (5 μM) (n = 4/group).

(D) *cFos* (immediate-early gene) transcript levels in hypothalamus cell lysates of A485- vs. vehicle-treated mice 1 h post-injection (n = 8/group).

(E) Representative immunostaining of cFos in the PVN. "3V" denotes third ventricle.

(F) Circulating ACTH concentration 1 h after A485 or vehicle injection (n = 8/group).

(G) A485 abundance in hypothalamus ("hypo") lysates or lysates of the brain excluding the hypothalamus ("brain") measured by LC-MS/MS and normalized according to tissue weight (n = 4/group).

(H) Glucose levels 45 min following A485 or vehicle administration (n = 3/group).

(I) Rectal body temperature across the three indicated conditions 2 h after injection (n = 3–4/group).

(J) CORT levels in the same mice.

(K) CORT serum concentration in response to A485 or vehicle challenge in mice with (RTX) or without (DMSO) ablation of TRPV1$^+$ sensory neurons measured by ELISA. Blood was collected 2 h post challenge (n = 3–4/group).

(L) Circulating CORT levels in A485- or vehicle-treated mice 2 h following exposure to the respective substances. A subset of mice (+) received ketamine/xylazine (ket/xyl) anesthesia prior to the challenge (n = 3–4/group).

(M) Serum concentration of CORT in mice injected i.v. with kappa bungarotoxin (kBTX) or PBS 15 min prior to A485 or vehicle challenge. Blood was collected at 2 h post-injection (n = 4–5/group). Data are presented as mean ± SEM. *p < 0.05, **p < 0.01, ***p < 0.001, ****p < 0.0001.

(A and K) Two-way ANOVA with Holm-Sidak's post hoc test (C, I, J, L, and M) one-way ANOVA with Holm-Sidak's post hoc test.

(D, F, and H) unpaired, two-tailed Student's t test.

convey peripheral A485 distribution to the CNS. We hypothesized that such fibers are cholinergic and likely carried by the vagus nerve because most viscera receive sensory innervation via this route.[56] Vagal ganglia mainly express nicotinic acetylcholine receptors containing the α3-subunit (nAchRα3), which are sensitive to inhibition by kappa bungarotoxin (kBTX), a snake venom.[57,58] kBTX has high affinity for α3, but not other nAchRs.[59] We found that nAchRα3 blockade by kBTX also did not prevent A485-induced CORT release (Figure 5M).

We conclude that A485 elicits central activation of the HPA axis via an indirect pathway that remains unknown.

HPA-axis activity relays the A485 leukocyte response independently of glucocorticoids

GCs are the main effectors of the HPA axis. To study the contributions of GC to A485-induced bone marrow mobilization, we used several orthogonal tools. First, we blocked the GC receptor pharmacologically (mifepristone/RU486) and genetically (*Nr3c1*$^{fl/fl}$ Rosa26CreERT2, referred to as *Nr3c1*^{KO}), both of which did not affect leukocyte populations in response to A485 (Figures 6A and S8A–S8C). Second, induction of GC deficiency failed to prevent increases in leukocytes (Figures 6B and S8D). Third, we subjected mice to adrenalectomy (ADX) or sham surgery, which successfully resulted in adrenal insufficiency as indicated by diminished systemic CORT abundance and a counterregulatory surge in ACTH levels (Figures S8E and S8F). ADX did not abrogate leuko- and lymphocytosis or neutrophilia (Figures 6C and S8G), demonstrating that GC, mineralocorticoids, and systemically released catecholamines are dispensable for the effects of A485 on leukocytes. By contrast, ADX mice exhibited even higher leukocyte counts than sham-controls (Figures 6C and S8G), implying that loss of HPA feedback supports the A485 leukocyte response. Therefore, we reasoned that the signal mediating the drug's effect on leukocytes derives from the CNS and is induced upon loss of HPA feedback. We hypothesized that this signal is ACTH because, unlike CRH, it is secreted into the systemic circulation,[60] where it can reach peripheral tissues such as the bone marrow.

Pharmacological inhibition of corticotropin-releasing hormone receptor 1 (CRHR1), which is upstream of ACTH (Figure 5B) and highly expressed in the brain but not in the bone or bone marrow (Figure S8H), by two independent small molecules (dmp696 and antalarmin) prevented A485-induced leukocytosis and neutrophilia (Figures 6D, 6E, S8I, and S8J). When we supplemented mice with recombinant ACTH (rACTH) in the presence of CRHR1 inhibition, neutrophils increased again (Figures 6F and 6G). We further noted that WT mice treated with rACTH developed neutrophilia, which was maintained upon disrupted GC signaling (Figures 6H, 6J, and S8K). By contrast, lymphopenia was lost when GCs were blocked (Figure 6J), demonstrating that neutrophils and lymphocytes are controlled by divergent effector mechanisms of the HPA axis.

In the murine bone marrow, transcriptional expression of the high-affinity ACTH receptor melanocortin receptor 2 (*Mc2r*) together with other melanocortin receptors was detected (Figure S9A). Both CD31^{+} and CD31^{-} bone marrow cells expressed Mc2r (Figure S9A), although at lower levels than the AT (Figure S9B), for which direct ACTH effects have previously been described.[61]

To narrow down the bone marrow cell type that may potentially be targeted by ACTH, we screened two publicly available single-cell RNA sequencing datasets. We found that Mc2r was expressed by the stroma but not hematopoietic precursor cells or mature leukocytes (Figures S9C and S9D). Within the bone marrow stroma, Mc2r transcripts were confined to the leptin-receptor-positive mesenchymal stromal cell population (LepR^{+} MSCs) (Figure S9D), the main endogenous source of CXCL12.[62] Consistent with these observations, blockade of CRHR1 was sufficient to increase bone marrow CXCL12 protein levels in A485-treated mice (Figure S9E). These data imply that the bone marrow is ACTH responsive.

In summary, our results show that central activation of the HPA axis by A485 relays leukocyte mobilization via CRHR1-regulated signals including ACTH, but independently of GCs. Given the pharmacodynamic profile of A485 and its potential to augment host defenses, we propose the generic name "prohiberin" (from latin "*prohibere*," to defend) for future studies investigating this compound.

DISCUSSION

With this study, we introduce the inhibition of the CBP/p300 HAT domain by the small-molecule A485 (prohiberin) as a mechanism to elicit acute and transient bone marrow mobilization, which is equally effective as G-CSF in mice. Although we found that A485-induced neutrophil mobilization depended on endogenous G-CSF activity, the pharmacodynamic effects of A485 and G-CSF treatment are distinct: first, neutrophilia onset is faster with A485 compared with G-CSF. Second, A485 neutrophilia requires CRHR1 but not GC, muscarinic receptors, or nociceptive nerves, all of which are involved in the G-CSF-mediated bone marrow response.[10,63] Third, B lymphocytes are mobilized by A485 but not G-CSF. Fourth, the SNS is not involved in relaying bone marrow mobilization by A485, while it is an important component of the G-CSF effector cascade,[7] and fifth, our results collectively suggest that CBP/p300 HAT activity is upstream, rather than downstream of CSF3R. Consistent with these observations, combining A485 and G-CSF resulted in superior neutrophil mobilization compared with treatment with either agent alone. We conclude that A485 requires endogenous G-CSF to evoke neutrophilia but engages additional effector pathways that are G-CSF independent.

We also noted that the effects of A485 on the bone marrow were shorter than those of G-CSF, which manifested as lower cell counts by 24 h post-injection. This difference between the two drugs has two important implications: On the one hand, A485 may be favored in cases where only short bursts of neutrophil mobilization are required such as in acute infection. In fact, unresolved monocytosis and neutrophilia can be detrimental in this context due to the risk of excessive inflammation and collateral tissue damage.[13,50] On the other hand, G-CSF could be superior to A485 in promoting long-term hematopoietic recovery. In our study, we did not find evidence for an acute effect of A485 on HSCs. However, this does not preclude the possibility, that repeated injections of A485 alone or in combination with G-CSF elicit mobilization of these cells. These avenues deserve to be explored in the future.

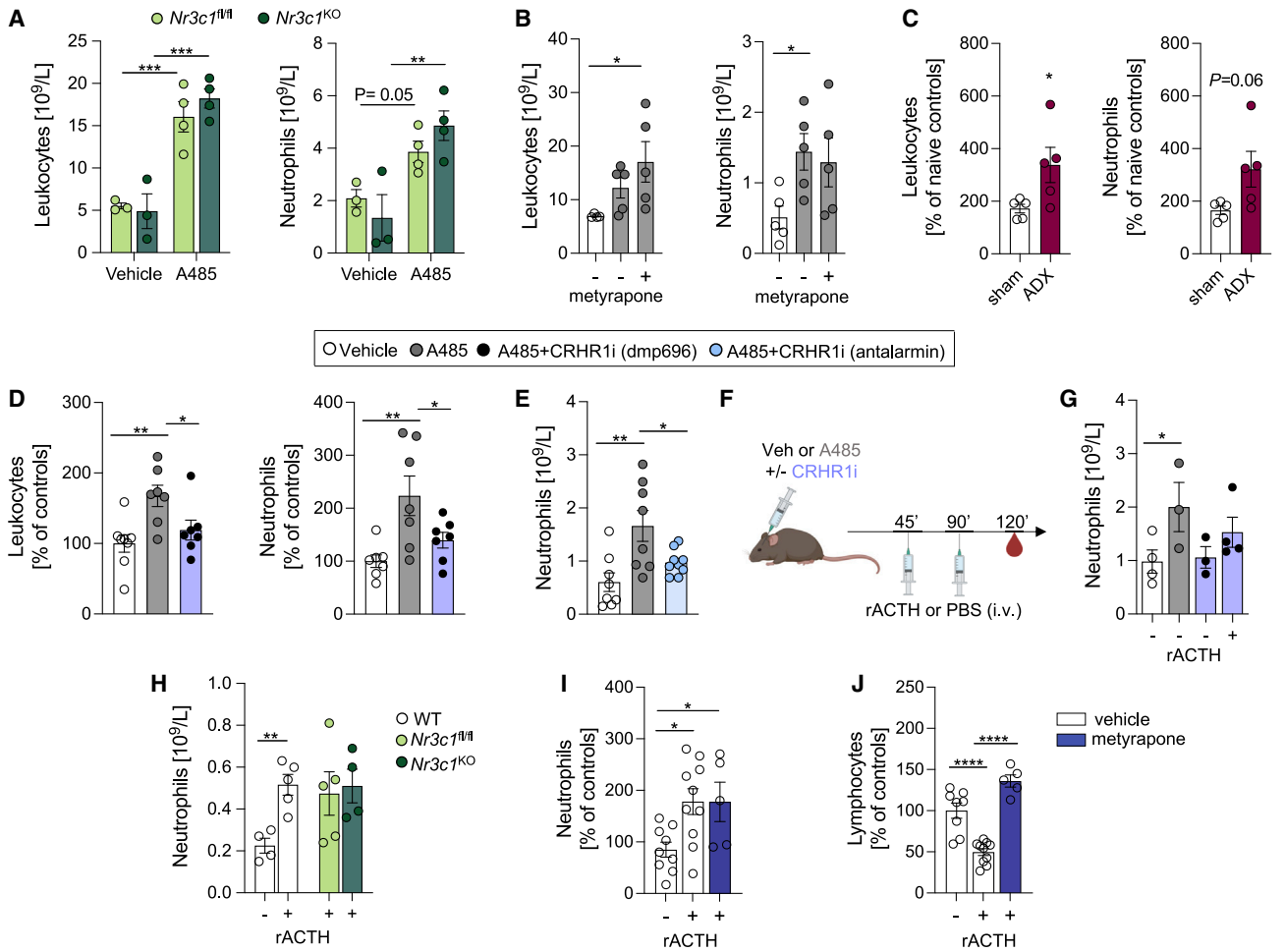

Figure 6. HPA-axis activity relays the A485 leukocyte response independently of glucocorticoids

(A) Quantification of leukocytes and neutrophils in the blood of A485- or vehicle-treated mice with ($Nr3c1^{Rosa26CreERT2}$, referred to as $Nr3c1^{KO}$) or without ($Nr3c1^{fl/fl}$) inducible global GC receptor (encoded by *Nr3c1*) deletion (n = 3–4/group).

(B) Leukocytes and neutrophils in A485- or vehicle-treated mice with (+) or without (–) pharmacologically induced GC deficiency by metyrapone (n = 5/group).

(C) Leukocytes and neutrophils in the blood of ADX- or sham-operated animals treated with A485 for 5 h. Results are expressed as percentage of naive controls (n = 5/group).

(D) Blood leukocytes and neutrophils in mice exposed to the indicated treatments. CRHR1i denotes a corticotropin-releasing hormone receptor 1 inhibitor (Dmp696). Results are expressed as percentage of vehicle controls (n = 7–8/group).

(E) Validation of the result from (D) using a second CRHR1i (antalarmin) (n = 8/group). Blood was collected 2 h following drug injection.

(F and G) (F) Experimental design (G) Neutrophils in vehicle-, A485-, or A485+CRHR1i-treated mice supplemented with (+) or without (–) recombinant ACTH (n = 3–4/group).

(H) Number of neutrophils in the blood of WT (C57BL/6J), $Nr3c1^{fl/fl}$, or $Nr3c1^{KO}$ mice 2 h following injection of rACTH (+) or vehicle (–) (experimental design akin to F) (n = 4–5/group).

(I and J) Blood neutrophils and total lymphocytes in mice treated with rACTH (+) or vehicle (–) in the presence (blue) or absence (white) of pharmacologically induced GC deficiency by metyrapone (n = 5–10/group) Data are presented as mean ± SEM. *p < 0.05, **p < 0.01, ***p < 0.001, ****p < 0.0001.

(A) Two-way ANOVA with Holm-Sidak's post hoc test.

(B, D–G, I, and J) One-way ANOVA with Holm-Sidak's post hoc test (C and H) unpaired, two-tailed Student's t test.

We infer that A485 might be introduced as a complementary pharmacological strategy to G-CSF derivatives in the clinics with potential benefits for rapid and short-term modulation of leukocyte compartments. Specifically, individuals suffering from acute neutropenic fever, in whom G-CSF supplementation does not confer clear clinical benefits,[21] may be a candidate population for A485 treatment. However, the therapeutic window of the drug needs to be better defined, as we only focused on a single time point post-infection. Accordingly, we do not know whether A485 treatment also confers benefits at later stages of the infection. This aspect is critical because patients typically present at variable stages of sepsis in the clinics, corresponding to a much more heterogeneous population than rodents, in which the onset of infection is clear to the investigator. Further, we only explored the effects of A485 in experimental listeriosis, a standard murine sepsis model, but whether the drug exerts protective effects in other bacterial and/or viral infections remains to be assessed. Another important consideration of

A485 therapy is the trade-off between augmentation of host defenses and immunopathology,[64,65] which could be dose limiting and needs to be rigorously characterized in preclinical models.

From a broader perspective, the established anti-tumor effects of A485[29,66,67] together with the herein reported immune modulation render the use of the compound attractive in the adjuvant setting of cancer therapy, where combating infectious complications and interference with (residual) malignant growth are both desirable. Vice versa, it is unknown whether inhibition of the CBP/p300 HAT domain can also exert pro-tumorigenic effects under certain conditions, but the bulk of available experimental data[29,66,67] argues against this notion.

The shifts in leukocyte populations induced by A485 reported in this study are unique because other types of challenges that promote HPA-axis activation (e.g., psychological stress) as well as the delivery of exogenous GC drive opposing movements of leukocyte subsets characterized by increases in blood neutrophils and concurrent lymphocyte migration into the bone marrow, which culminates in lymphopenia.[13,50] We observed similar changes when ACTH was injected into GC-competent animals, and lymphopenia but not neutrophilia was lost when GCs were blocked. Lymphocyte homing into the bone marrow is strongly shaped by CXCR4, the expression of which is typically augmented when GC levels rise.[68] By contrast, A485 triggers HPA-axis activity while simultaneously suppressing CXCR4 transcription, inhibiting the production of the receptor's ligand (CXCL12) and downregulating a key downstream effector molecule, VLA4. Our data suggest that some of these changes result from a direct effect of the drug on the bone marrow, which could explain lymphocyte egress into the blood despite high levels of GC.

ACTH is sufficient to evoke neutrophilia in patients suffering from adrenal insufficiency, who have a diminished GC response.[69] In rodents, ADX, but not sham surgery, is linked to neutrophilia.[70] Likewise, high ACTH levels in subclinical Cushing's syndrome can be associated with substantial neutrophilia, even if cortisol levels are only minimally elevated.[71] Consistent with these observations, we found that ACTH promoted increases in neutrophils in the absence of functional GC signaling. These observations support a role of ACTH in controlling neutrophil compartments and raise the question which other homeostatic functions classically attributed to GC are partly or fully mediated by its upstream regulator ACTH. Such GC-independent functions of ACTH are reminiscent of those of other pituitary hormones, which can directly affect organ physiology independent of the gland-derived endocrine mediators that they control.[72,73] The relatively low expression of MC2R in the murine bone marrow suggests that ACTH signaling may not occur in the steady state in this tissue. Instead, a certain threshold of HPA-axis activation and ACTH release may be required to engage bone marrow MC2Rs. This could imply that ACTH modulates leukocyte compartments only upon stress, injury, or other types of insults, where bone marrow mobilization is a physiological response.

Lastly, although G-CSF activates the HPA axis,[10] the reciprocal pathway in which ACTH regulates G-CSF biology should be further investigated. Understanding how ACTH controls leukocyte compartments and the hematopoietic stem cell niche is thus an exciting field for scientific discoveries.

Limitations of the study

We currently do not know how A485 activates the HPA axis at the hypothalamic level. We suspect that soluble signals or afferent neuronal inputs (TRPV1$^-$ and non-cholinergic) mediate the drug's effect on the PVN. Likewise, the intracellular signaling and effector machinery (beyond integrins) driving leukocyte release from the bone marrow in response to A485 require further mechanistic investigations, which is outside the scope of this study. We also cannot foresee the biological consequences of chronic, repeated A485 exposure, although our data argue that such dosing regimens may not be required to achieve therapeutic effects. We further did not include *Ep300*-, *Crebbp*-deficient, or double-mutant mice in our study, which renders bone marrow mobilization by A485 potentially CBP/p300-independent ("off-target"). We did not perform these experiments because (1) homozygous deletion of either protein is embryonically lethal,[74] (2) heterozygous deletion of *Crebbp* or *Ep300* can be compensated by its respective ortholog,[75] and (3) available genetic models are not HAT specific and thus result in severe phenotypes due to the vital functions of Crebbp/p300 as transcriptional cofactors,[75,76] collectively limiting their experimental utility. Given that leukocytosis could be recapitulated with an independent CBP/HAT inhibitor with a chemically distinct structure (non-spirocyclic), we believe that the probability for an off-target mechanism of action is low. However, we cannot rule out an off-target mechanism with our current set of data. Moreover, the paucity of a genetic model prevented us from identifying which cell type(s) targeted by A485 are mainly responsible for leukocytosis in response to the drug. Our data suggest that cells both inside and outside the bone marrow convey these effects. Finally, pathways other than ACTH signaling that are under control of CRHR1 must contribute to A485-induced leukocytosis and neutrophilia because supplementation of ACTH failed to fully recover cell numbers in the context of CRHR1 inhibition.

STAR★METHODS

Detailed methods are provided in the online version of this paper and include the following:

- KEY RESOURCES TABLE
- RESOURCE AVAILABILITY
  - Lead contact
  - Materials availability
  - Data and code availability
- EXPERIMENTAL MODEL AND STUDY PARTICIPANTS DETAILS
  - Mice
  - Human study participants
  - Bone marrow cultures and murine bone marrow derived macrophage (mBMDM) differentiation
  - Y1 cell culture
- METHOD DETAILS
  - Drugs and treatments
  - Listeria monocytogenes infection and quantification of bacterial burden
  - Intravascular leukocyte labeling

- Cell tracking
- Conventional and automated flow cytometry analysis
- Hypothalamic explants
- A485 measurements
- Ablation of TRPV1+ sensory neurons
- Acetyl CoA quantification
- CXCL12 migration assay
- Magnetic-assisted cell sorting (MACS)
- Quantitative polymerase chain reaction (qPCR)
- Protein isolation and immunoblotting
- Enzyme-linked sorbent assays (ELISAs)
- Sublethal Irradiation
- Immunofluorescence analysis
- LDH release assay
- Organ toxicity screen

● QUANTIFICATION AND STATISTICAL ANALYSIS

SUPPLEMENTAL INFORMATION

Supplemental information can be found online at https://doi.org/10.1016/j.immuni.2024.01.005.

ACKNOWLEDGMENTS

We thank all members of the Bone Lab and Wang Lab for helpful discussions. We also thank Dr. Simon Schenk for providing feedback on CBP/p300 pharmacology. We thank Dr. Joao Pereira and Dr. Takeshi Ito for their help with the migration assay, Dr. Richard Locksley for providing the YRS ST2/IL-25/TSLPR TKO mice, and Dr. Jan Tuckermann for sharing the floxed Nr3c1 animals. We thank Dr. Ruslan Medzhitov for providing the *Listeria monocytogenes* strain and Dr. Charlotte Steenblock for sharing Y-1 cells. This work was funded by a Walter Benjamin Program Post-Doctoral Fellowship (JA-3511/2-1, project no. 525808956) by the German Research Foundation (awarded to N.P.J.); a start-up grant by the German Society of Endocrinology (awarded to N.P.J.), the Mildred-Scheel-Nachwuchszentrum of the German Cancer Aid (grant: 70113306 to T.D.R. and A.G.), the μBone Schwerpunktprogramm (2084) of the German Research Foundation (to T.D.R., A.G., L.C.H., and M.R.), the FerOs program of the German Research Foundation (to L.C.H. and M.R.), the Emmy Noether Program of the German Research Foundation (SCHE1645/2-1) (to C.S.), the European Research Council (ERC) (635872) (to C.S.), the National Institutes of Health (R01 AI162645 and R01 AR080104 to A.W.), the Smith Family Foundation (to A.W.), and the Pew Charitable Trusts (to A.W.).

AUTHOR CONTRIBUTIONS

Conceptualization, N.P.J., T.D.R., C.S., and A.W.; data acquisition, N.P.J., D.B., M.H., U.B., S.P., R.O., S.T., T.G., F.S., M.S., C.Z., and T.M.Y.; data analysis, N.P.J., D.B., M.H., R.O., S.T., T.G., F.S., and M.S.; methodology, N.P.J., U.B., R.O., S.T., M.S., T.G., F.S., T.M.Y., H.W., and C.Z.; supervision, N.P.J., T.D.R., C.S., and A.W.; manuscript writing, N.P.J., C.S., T.D.R., and A.W.; manuscript editing, N.P.J., C.S., T.D.R., A.W., M.H., U.B., R.O., S.P., S.T., T.G., F.S., A.B., M.S., H.B., W.C.P., F.K.S., A.G., L.C.H., and M.R.

DECLARATION OF INTERESTS

N.P.J. is an inventor of a patent filed by the Technical University of Dresden that describes the medical use of HAT inhibitors for bone marrow mobilization and the treatment of neutropenia. T.D.R., L.C.H., and C.S. are co-inventors of this patent.

Received: June 29, 2023
Revised: December 1, 2023
Accepted: January 8, 2024
Published: January 31, 2024

REFERENCES

1. Calvi, L.M., and Link, D.C. (2015). The hematopoietic stem cell niche in homeostasis and disease. Blood *126*, 2443–2451.
2. Méndez-Ferrer, S., Lucas, D., Battista, M., and Frenette, P.S. (2008). Haematopoietic stem cell release is regulated by circadian oscillations. Nature *452*, 442–447.
3. Pick, R., He, W., Chen, C.S., and Scheiermann, C. (2019). Time-of-Day-Dependent Trafficking and Function of Leukocyte Subsets. Trends Immunol. *40*, 524–537.
4. Nicolás-Ávila, J.Á., Adrover, J.M., and Hidalgo, A. (2017). Neutrophils in Homeostasis, Immunity, and Cancer. Immunity *46*, 15–28.
5. Manz, M.G., and Boettcher, S. (2014). Emergency granulopoiesis. Nat. Rev. Immunol. *14*, 302–314.
6. Santos, I., Colaço, H.G., Neves-Costa, A., Seixas, E., Velho, T.R., Pedroso, D., Barros, A., Martins, R., Carvalho, N., Payen, D., et al. (2020). CXCL5-mediated recruitment of neutrophils into the peritoneal cavity of Gdf15-deficient mice protects against abdominal sepsis. Proc. Natl. Acad. Sci. USA *117*, 12281–12287.
7. Katayama, Y., Battista, M., Kao, W.M., Hidalgo, A., Peired, A.J., Thomas, S.A., and Frenette, P.S. (2006). Signals from the sympathetic nervous system regulate hematopoietic stem cell egress from bone marrow. Cell *124*, 407–421.
8. Lucas, D., Scheiermann, C., Chow, A., Kunisaki, Y., Bruns, I., Barrick, C., Tessarollo, L., and Frenette, P.S. (2013). Chemotherapy-induced bone marrow nerve injury impairs hematopoietic regeneration. Nat. Med. *19*, 695–703.
9. Druzd, D., Matveeva, O., Ince, L., Harrison, U., He, W., Schmal, C., Herzel, H., Tsang, A.H., Kawakami, N., Leliavski, A., et al. (2017). Lymphocyte Circadian Clocks Control Lymph Node Trafficking and Adaptive Immune Responses. Immunity *46*, 120–132.
10. Pierce, H., Zhang, D., Magnon, C., Lucas, D., Christin, J.R., Huggins, M., Schwartz, G.J., and Frenette, P.S. (2017). Cholinergic Signals from the CNS Regulate G-CSF-Mediated HSC Mobilization from Bone Marrow via a Glucocorticoid Signaling Relay. Cell Stem Cell *20*, 648–658.e4.
11. Crespo, M., Gonzalez-Teran, B., Nikolic, I., Mora, A., Folgueira, C., Rodríguez, E., Leiva-Vega, L., Pintor-Chocano, A., Fernández-Chacón, M., Ruiz-Garrido, I., et al. (2020). Neutrophil infiltration regulates clock-gene expression to organize daily hepatic metabolism. eLife *9*.
12. Hanoun, M., Maryanovich, M., Arnal-Estapé, A., and Frenette, P.S. (2015). Neural regulation of hematopoiesis, inflammation, and cancer. Neuron *86*, 360–373.
13. Poller, W.C., Downey, J., Mooslechner, A.A., Khan, N., Li, L., Chan, C.T., McAlpine, C.S., Xu, C., Kahles, F., He, S., et al. (2022). Brain motor and fear circuits regulate leukocytes during acute stress. Nature *607*, 578–584.
14. McAlpine, C.S., Kiss, M.G., Rattik, S., He, S., Vassalli, A., Valet, C., Anzai, A., Chan, C.T., Mindur, J.E., Kahles, F., et al. (2019). Sleep modulates haematopoiesis and protects against atherosclerosis. Nature *566*, 383–387.
15. Cossío, I., Lucas, D., and Hidalgo, A. (2019). Neutrophils as regulators of the hematopoietic niche. Blood *133*, 2140–2148.
16. Li, J.H., Hepworth, M.R., and O'Sullivan, T.E. (2023). Regulation of systemic metabolism by tissue-resident immune cell circuits. Immunity *56*, 1168–1186.
17. Wiedemann, S.J., Trimigliozzi, K., Dror, E., Meier, D.T., Molina-Tijeras, J.A., Rachid, L., Le Foll, C., Magnan, C., Schulze, F., Stawiski, M., et al. (2022). The cephalic phase of insulin release is modulated by IL-1β. Cell Metab. *34*, 991–1003.e6.
18. Karpova, D., Rettig, M.P., Ritchey, J., Cancilla, D., Christ, S., Gehrs, L., Chendamarai, E., Evbuomwan, M.O., Holt, M., Zhang, J., et al. (2019). Targeting VLA4 integrin and CXCR2 mobilizes serially repopulating hematopoietic stem cells. J. Clin. Invest. *129*, 2745–2759.
19. Mehta, H.M., Malandra, M., and Corey, S.J. (2015). G-CSF and GM-CSF in Neutropenia. J. Immunol. *195*, 1341–1349.

20. Frampton, J.E., Lee, C.R., and Faulds, D. (1994). Filgrastim. A review of its pharmacological properties and therapeutic efficacy in neutropenia. Drugs *48*, 731–760.

21. Mhaskar, R., Clark, O.A., Lyman, G., Engel Ayer Botrel, T., Morganti Paladini, L., and Djulbegovic, B. (2014). Colony-stimulating factors for chemotherapy-induced febrile neutropenia. Cochrane Database Syst. Rev. *2014*, CD003039.

22. Wang, Y., Chen, L., Liu, F., Zhao, N., Xu, L., Fu, B., and Li, Y. (2019). Efficacy and tolerability of granulocyte colony-stimulating factors in cancer patients after chemotherapy: A systematic review and Bayesian network meta-analysis. Sci. Rep. *9*, 15374.

23. Jaschke, N.P., and Rachner, T.D. (2023). Cancer cachexia as a blueprint for treating obesity. Trends Endocrinol. Metab. *34*, 395–403.

24. Skokowa, J., Dale, D.C., Touw, I.P., Zeidler, C., and Welte, K. (2017). Severe congenital neutropenias. Nat. Rev. Dis. Primers *3*, 17032.

25. Beekman, R., Valkhof, M.G., Sanders, M.A., van Strien, P.M., Haanstra, J.R., Broeders, L., Geertsma-Kleinekoort, W.M., Veerman, A.J., Valk, P.J., Verhaak, R.G., et al. (2012). Sequential gain of mutations in severe congenital neutropenia progressing to acute myeloid leukemia. Blood *119*, 5071–5077.

26. Cheng, G., Liu, F., Asai, T., Lai, F., Man, N., Xu, H., Chen, S., Greenblatt, S., Hamard, P.J., Ando, K., et al. (2017). Loss of p300 accelerates MDS-associated leukemogenesis. Leukemia *31*, 1382–1390.

27. Kasper, L.H., Boussouar, F., Ney, P.A., Jackson, C.W., Rehg, J., van Deursen, J.M., and Brindle, P.K. (2002). A transcription-factor-binding surface of coactivator p300 is required for haematopoiesis. Nature *419*, 738–743.

28. Ogryzko, V.V., Schiltz, R.L., Russanova, V., Howard, B.H., and Nakatani, Y. (1996). The transcriptional coactivators p300 and CBP are histone acetyltransferases. Cell *87*, 953–959.

29. Lasko, L.M., Jakob, C.G., Edalji, R.P., Qiu, W., Montgomery, D., Digiammarino, E.L., Hansen, T.M., Risi, R.M., Frey, R., Manaves, V., et al. (2017). Discovery of a selective catalytic p300/CBP inhibitor that targets lineage-specific tumours. Nature *550*, 128–132.

30. Dekker, F.J., van den Bosch, T., and Martin, N.I. (2014). Small molecule inhibitors of histone acetyltransferases and deacetylases are potential drugs for inflammatory diseases. Drug Discov. Today *19*, 654–660.

31. Hammitzsch, A., Tallant, C., Fedorov, O., O'Mahony, A., Brennan, P.E., Hay, D.A., Martinez, F.O., Al-Mossawi, M.H., de Wit, J., Vecellio, M., et al. (2015). CBP30, a selective CBP/p300 bromodomain inhibitor, suppresses human Th17 responses. Proc. Natl. Acad. Sci. USA *112*, 10768–10773.

32. Gibson, C., and Berliner, N. (2014). How we evaluate and treat neutropenia in adults. Blood *124*, 1251–1258.

33. Lucas, D., Battista, M., Shi, P.A., Isola, L., and Frenette, P.S. (2008). Mobilized hematopoietic stem cell yield depends on species-specific circadian timing. Cell Stem Cell *3*, 364–366.

34. Karpova, D., Ritchey, J.K., Holt, M.S., Abou-Ezzi, G., Monlish, D., Batoon, L., Millard, S., Spohn, G., Wiercinska, E., Chendamarai, E., et al. (2017). Continuous blockade of CXCR4 results in dramatic mobilization and expansion of hematopoietic stem and progenitor cells. Blood *129*, 2939–2949.

35. Wiley, S., Swayne, S., Rubinstein, J.H., Lanphear, N.E., and Stevens, C.A. (2003). Rubinstein-Taybi syndrome medical guidelines. Am. J. Med. Genet. A *119A*, 101–110.

36. Lee, Y.R., Lin, Y.C., Chang, Y.H., Huang, H.Y., Hong, Y.K., Aala, W.J.F., Tu, W.T., Tsai, M.C., Chou, Y.Y., and Hsu, C.K. (2022). Genetic Diagnosis of Rubinstein-Taybi Syndrome With Multiplex Ligation-Dependent Probe Amplification (MLPA) and Whole-Exome Sequencing (WES): Case Series With a Novel CREBBP Variant. Front. Genet. *13*, 848879.

37. Welsh, C., Welsh, P., Mark, P.B., Celis-Morales, C.A., Lewsey, J., Gray, S.R., Lyall, D.M., Iliodromiti, S., Gill, J.M.R., Pell, J., et al. (2018). Association of Total and Differential Leukocyte Counts With Cardiovascular Disease and Mortality in the UK Biobank. Arterioscler. Thromb. Vasc. Biol. *38*, 1415–1423.

38. Buoro, S., Carobene, A., Seghezzi, M., Manenti, B., Pacioni, A., Ceriotti, F., Ottomano, C., and Lippi, G. (2017). Short- and medium-term biological variation estimates of leukocytes extended to differential count and morphology-structural parameters (cell population data) in blood samples obtained from healthy people. Clin. Chim. Acta *473*, 147–156.

39. Caggiano, V., Weiss, R.V., Rickert, T.S., and Linde-Zwirble, W.T. (2005). Incidence, cost, and mortality of neutropenia hospitalization associated with chemotherapy. Cancer *103*, 1916–1924.

40. Vento, S., and Cainelli, F. (2003). Infections in patients with cancer undergoing chemotherapy: aetiology, prevention, and treatment. Lancet Oncol. *4*, 595–604.

41. López, S., Marco, A.J., Prats, N., and Czuprynski, C.J. (2000). Critical role of neutrophils in eliminating Listeria monocytogenes from the central nervous system during experimental murine listeriosis. Infect. Immun. *68*, 4789–4791.

42. Sender, R., Weiss, Y., Navon, Y., Milo, I., Azulay, N., Keren, L., Fuchs, S., Ben-Zvi, D., Noor, E., and Milo, R. (2023). The total mass, number, and distribution of immune cells in the human body. Proc. Natl. Acad. Sci. USA *120*, e2308511120.

43. Beck, T.C., Gomes, A.C., Cyster, J.G., and Pereira, J.P. (2014). CXCR4 and a cell-extrinsic mechanism control immature B lymphocyte egress from bone marrow. J. Exp. Med. *211*, 2567–2581.

44. Petty, J.M., Lenox, C.C., Weiss, D.J., Poynter, M.E., and Suratt, B.T. (2009). Crosstalk between CXCR4/stromal derived factor-1 and VLA-4/VCAM-1 pathways regulates neutrophil retention in the bone marrow. J. Immunol. *182*, 604–612.

45. Gazitt, Y., and Akay, C. (2004). Mobilization of myeloma cells involves SDF-1/CXCR4 signaling and downregulation of VLA-4. Stem Cells *22*, 65–73.

46. Weber, G.F., Chousterman, B.G., He, S., Fenn, A.M., Nairz, M., Anzai, A., Brenner, T., Uhle, F., Iwamoto, Y., Robbins, C.S., et al. (2015). Interleukin-3 amplifies acute inflammation and is a potential therapeutic target in sepsis. Science *347*, 1260–1265.

47. Schneidawind, C., Jahnke, S., Schober-Melms, I., Schumm, M., Handgretinger, R., Faul, C., Kanz, L., Bethge, W., and Schneidawind, D. (2019). G-CSF administration prior to donor lymphocyte apheresis promotes anti-leukaemic effects in allogeneic HCT patients. Br. J. Haematol. *186*, 60–71.

48. Scheiermann, C., Kunisaki, Y., Lucas, D., Chow, A., Jang, J.E., Zhang, D., Hashimoto, D., Merad, M., and Frenette, P.S. (2012). Adrenergic nerves govern circadian leukocyte recruitment to tissues. Immunity *37*, 290–301.

49. Nakagawa, M., Terashima, T., D'yachkova, Y., Bondy, G.P., Hogg, J.C., and van Eeden, S.F. (1998). Glucocorticoid-induced granulocytosis: contribution of marrow release and demargination of intravascular granulocytes. Circulation *98*, 2307–2313.

50. Janssen, H., Kahles, F., Liu, D., Downey, J., Koekkoek, L.L., Roudko, V., D'Souza, D., McAlpine, C.S., Halle, L., Poller, W.C., et al. (2023). Monocytes re-enter the bone marrow during fasting and alter the host response to infection. Immunity *56*, 783–796.e7.

51. Jaschke, N.P. (2022). Control loop designs in health and disease. Nat. Rev. Endocrinol. *18*, 653–654.

52. Wagoner, P.K., and Pallotta, B.S. (1988). Modulation of acetylcholine receptor desensitization by forskolin is independent of cAMP. Science *240*, 1655–1657.

53. Jais, A., and Brüning, J.C. (2022). Arcuate Nucleus-Dependent Regulation of Metabolism-Pathways to Obesity and Diabetes Mellitus. Endocr. Rev. *43*, 314–328.

54. Qing, H., Desrouleaux, R., Israni-Winger, K., Mineur, Y.S., Fogelman, N., Zhang, C., Rashed, S., Palm, N.W., Sinha, R., Picciotto, M.R., et al. (2020). Origin and Function of Stress-Induced IL-6 in Murine Models. Cell *182*, 372–387.e14.

55. Mastorakos, G., Chrousos, G.P., and Weber, J.S. (1993). Recombinant interleukin-6 activates the hypothalamic-pituitary-adrenal axis in humans. J. Clin. Endocrinol. Metab. *77*, 1690–1694.

56. Berthoud, H.R., and Neuhuber, W.L. (2000). Functional and chemical anatomy of the afferent vagal system. Auton. Neurosci. *85*, 1–17.

57. Chiappinelli, V.A. (1983). Kappa-bungarotoxin: a probe for the neuronal nicotinic receptor in the avian ciliary ganglion. Brain Res. *277*, 9–22.

58. Bibevski, S., Zhou, Y., McIntosh, J.M., Zigmond, R.E., and Dunlap, M.E. (2000). Functional nicotinic acetylcholine receptors that mediate ganglionic transmission in cardiac parasympathetic neurons. J. Neurosci. *20*, 5076–5082.

59. Grant, G.A., Luetje, C.W., Summers, R., and Xu, X.L. (1998). Differential roles for disulfide bonds in the structural integrity and biological activity of kappa-Bungarotoxin, a neuronal nicotinic acetylcholine receptor antagonist. Biochemistry *37*, 12166–12171.

60. Veldhuis, J.D., Iranmanesh, A., Naftolowitz, D., Tatham, N., Cassidy, F., and Carroll, B.J. (2001). Corticotropin secretory dynamics in humans under low glucocorticoid feedback. J. Clin. Endocrinol. Metab. *86*, 5554–5563.

61. van den Beukel, J.C., Grefhorst, A., Quarta, C., Steenbergen, J., Mastroberardino, P.G., Lombès, M., Delhanty, P.J., Mazza, R., Pagotto, U., van der Lely, A.J., et al. (2014). Direct activating effects of adrenocorticotropic hormone (ACTH) on brown adipose tissue are attenuated by corticosterone. FASEB J. *28*, 4857–4867.

62. Ding, L., Saunders, T.L., Enikolopov, G., and Morrison, S.J. (2012). Endothelial and perivascular cells maintain haematopoietic stem cells. Nature *481*, 457–462.

63. Gao, X., Zhang, D., Xu, C., Li, H., Caron, K.M., and Frenette, P.S. (2021). Nociceptive nerves regulate haematopoietic stem cell mobilization. Nature *589*, 591–596.

64. Okin, D., and Medzhitov, R. (2012). Evolution of inflammatory diseases. Curr. Biol. *22*, R733–R740.

65. Jaschke, N.P., Pählig, S., Sinha, A., Adolph, T.E., Colunga, M.L., Hofmann, M., Wang, A., Thiele, S., Schwärzler, J., Kleymann, A., et al. (2022). Dickkopf1 fuels inflammatory cytokine responses. Commun. Biol. *5*, 1391.

66. Wei, W., Song, Z., Chiba, M., Wu, W., Jeong, S., Zhang, J.P., Kadin, M.E., Nakagawa, M., and Yang, Y. (2023). Analysis and therapeutic targeting of the EP300 and CREBBP acetyltransferases in anaplastic large cell lymphoma and Hodgkin lymphoma. Leukemia *37*, 396–407.

67. Zhou, X.R., Li, X., Liao, L.P., Han, J., Huang, J., Li, J.C., Tao, H.R., Fan, S.J., Chen, Z.F., Li, Q., et al. (2022). P300/CBP inhibition sensitizes mantle cell lymphoma to PI3Kδ inhibitor idelalisib. Acta Pharmacol. Sin. *43*, 457–469.

68. Cain, D.W., Bortner, C.D., Diaz-Jimenez, D., Petrillo, M.G., Gruver-Yates, A., and Cidlowski, J.A. (2020). Murine Glucocorticoid Receptors Orchestrate B Cell Migration Selectively between Bone Marrow and Blood. J. Immunol. *205*, 619–629.

69. Hills, A.G., Forsham, P.H., and Finch, C.A. (1948). Changes in circulating leukocytes induced by the administration of pituitary adrenocorticotrophic hormone in man. Blood *3*, 755–768.

70. Cavalcanti, D.M., Lotufo, C.M., Borelli, P., Tavassi, A.M., Pereira, A.L., Markus, R.P., and Farsky, S.H. (2006). Adrenal deficiency alters mechanisms of neutrophil mobilization. Mol. Cell. Endocrinol. *249*, 32–39.

71. Zhang, Y., Lin, X., Liu, F., Shou, S., and Jin, H. (2023). Neutrophilia with subclinical Cushing's disease: A case report and literature review. Open Life Sci. *18*, 20220540.

72. Liu, P., Ji, Y., Yuen, T., Rendina-Ruedy, E., DeMambro, V.E., Dhawan, S., Abu-Amer, W., Izadmehr, S., Zhou, B., Shin, A.C., et al. (2017). Blocking FSH induces thermogenic adipose tissue and reduces body fat. Nature *546*, 107–112.

73. Sun, L., Peng, Y., Sharrow, A.C., Iqbal, J., Zhang, Z., Papachristou, D.J., Zaidi, S., Zhu, L.L., Yaroslavskiy, B.B., Zhou, H., et al. (2006). FSH directly regulates bone mass. Cell *125*, 247–260.

74. Kasper, L.H., Fukuyama, T., Biesen, M.A., Boussouar, F., Tong, C., de Pauw, A., Murray, P.J., van Deursen, J.M., and Brindle, P.K. (2006). Conditional knockout mice reveal distinct functions for the global transcriptional coactivators CBP and p300 in T-cell development. Mol. Cell. Biol. *26*, 789–809.

75. Martins, V.F., LaBarge, S.A., Stanley, A., Svensson, K., Hung, C.W., Keinan, O., Ciaraldi, T.P., Banoian, D., Park, J.E., Ha, C., et al. (2022). p300 or CBP is required for insulin-stimulated glucose uptake in skeletal muscle and adipocytes. JCI Insight *7*, e141344.

76. Holmstrom, S.R., Wijayatunge, R., McCrum, K., Mgbemena, V.E., and Ross, T.S. (2019). Functional Interaction of BRCA1 and CREBBP in Murine Hematopoiesis. iScience *19*, 809–820.

77. Shearer, W.T., Rosenblatt, H.M., Gelman, R.S., Oyomopito, R., Plaeger, S., Stiehm, E.R., Wara, D.W., Douglas, S.D., Luzuriaga, K., McFarland, E.J., et al. (2003). Lymphocyte subsets in healthy children from birth through 18 years of age: the Pediatric AIDS Clinical Trials Group P1009 study. J. Allergy Clin. Immunol. *112*, 973–980.

78. Baral, P., Umans, B.D., Li, L., Wallrapp, A., Bist, M., Kirschbaum, T., Wei, Y., Zhou, Y., Kuchroo, V.K., Burkett, P.R., et al. (2018). Nociceptor sensory neurons suppress neutrophil and γδ T cell responses in bacterial lung infections and lethal pneumonia. Nat. Med. *24*, 417–426.

79. Zhang, B., Ma, S., Rachmin, I., He, M., Baral, P., Choi, S., Gonçalves, W.A., Shwartz, Y., Fast, E.M., Su, Y., et al. (2020). Hyperactivation of sympathetic nerves drives depletion of melanocyte stem cells. Nature *577*, 676–681.

STAR★METHODS

KEY RESOURCES TABLE

REAGENT or RESOURCE	SOURCE	IDENTIFIER
Antibodies		
CD45R (B220) PE-Cyanine7 (clone RA3-6B2)	Thermo Fisher Sci.	Cat# 25-0452-82
CD45R (B220) biotin (clone RA3-6B2)	Thermo Fisher Sci.	Cat# 13-0452-82
CD45 BUV395 (clone 30-F11)	BD Pharmingen	Cat# 565967
CD3e APC (clone 145-2C11)	Thermo Fisher Sci.	Cat# 17-0031-82
CD3e biotin (clone 145-2C11)	Thermo Fisher Sci.	Cat# 13-0031-82
CD11b PE (clone M1/70)	Thermo Fisher Sci.	Cat# 12-0112-82
CD11b biotin (clone M1/70)	Thermo Fisher Sci.	Cat# 13-0118-82
CD16/32 A700 (clone 93)	Thermo Fisher Sci.	Cat# 56-0161-82
CD19 biotin (clone 1D3)	Thermo Fisher Sci.	Cat# 13-0193-82
CD41 PerCP eFluor 710 (clone MWReg30)	Thermo Fisher Sci.	Cat# 46-0411-82
CD45 PE (clone 3D-F11)	Thermo Fisher Sci.	Cat# 12-0451-82
CD48 FITC (clone HM48-1)	Biolegend	Cat# 11-0481-82
CD105 APC (clone 120414)	Biolegend	Cat# MJ7/18
CD106 FITC (clone 429)	Biolegend	Cat# 105705
CD49d PE (clone 9C10)	Biolegend	Cat# 103705
CD150 PE-Cyanine7 (clone TC15-12F12.2)	BioLegend	Cat# 115914
CD117 (c-Kit) APC-eFluor 780 (clone 2B8)	Thermo Fisher Sci.	Cat# 47-1171-82
CD117 (c-Kit) biotin (clone 2B8)	Thermo Fisher Sci.	Cat# 13-1171-85
Ly-6G/Ly-6C biotin (clone RB6-8C5)	Thermo Fisher Sci.	Cat# 13-5931-82
Ly-6G/Ly-6C eFluor 450 (clone RB6-8C5)	Thermo Fisher Sci.	Cat# 48-5931-82
NK1.1 biotin (clone PK136)	Thermo Fisher Sci.	Cat# 13-5941-82
Streptavidin eFluor 450	Thermo Fisher Sci.	Cat# 48-4317-82
Ly-6A/E (Sca-1) PE-Cyanine5 (clone D7)	Thermo Fisher Sci.	Cat# 15-5981-82
Ter-119 biotin (clone TER119)	Thermo Fisher Sci.	Cat# MA5-17819
CD45 PE-Cy7 (clone 30-F11)	eBioscience	Cat# 25-0451-82
CD45 APC (clone 30-F11)	BioLegend	Cat# 103112
CD45.1 FITC (clone A20)	eBioscience	Cat# 11-0453-81
CD45.2 PE-Cy7 (clone 104)	eBioscience	Cat# 25-0454-80
Ly6G AF700 (clone RB6-8C5)	eBioscience	Cat# 56-5931-82
Ly6G APC (clone RB6-8C5)	Biolegend	Cat# 108411
CD3 FITC (clone 17A2)	BD Pharmingen	Cat# 561798
CD3 eF450 (clone 17A2)	eBioscience	Cat# 48-0032-80
CD3 PE-Cy7 (clone 17A2)	Biolegend	Cat# 560591
CD19 PE (clone eBio1D3)	BD Pharmingen	Cat# 557399
CD19 APC (clone eBio1D3)	eBioscience	Cat# 17-0193-80
CD19 FITC (clone 1D3/CD19)	Biolegend	Cat# 152404
CD11b PerCP Cy5.5 (clone M1/70)	eBioscience	Cat# 45-0112-82
Cd11b PB (clone M1/70)	Biolegend	Cat# 101224
anti-H3	Cell Signaling Tech.	Cat# 9715
anti-H3K18ac	Cell Signaling Tech.	Cat# 9675
anti-Stat3	Cell Signaling Tech.	Cat# 9132
anti-stat3-phospho (Tyr705)	Cell Signaling Tech.	Cat# 9131
anti-cFos	Sigma Aldrich	Cat# F7799
Anti-rabbit Alexa 594	Thermo Fisher Sci.	Cat# **A-11012**

(*Continued on next page*)

Continued

REAGENT or RESOURCE	SOURCE	IDENTIFIER
rabbit anti-mouse G-csf	R&D	Cat# MAB414
rabbit IgG isotype control	R&D	Cat# MAB5005
Rat IgG2b isotype control clone LTF-2	BioXcell	Cat# BE0090
anti-mouse IL-6R clone 15A7	BioXcell	Cat # BE0047
Biological samples		
Human DNA	University of Milano Bicocca	N/A
Human blood	University of Milano Bicocca	N/A
Chemicals, peptides, and recombinant proteins		
A485	Medchemexpress	Cat# HY-107455
C646	Medchemexpress	Cat# HY-13823
SGC-CBP30	Medchemexpress	Cat# HY-15862
5-FU	Medchemexpress	Cat# HY-90006
Fingolimod	Medchemexpress	Cat# HY-11065
Forskolin	Medchemexpress	Cat# HY-15371
NU9056	Tocris	Cat# 4903
6-OHDA	Medchemexpress	Cat# HY-B1081
AMD3100	Medchemexpress	Cat# HY-10046
Firategrast	Medchemexpress	Cat# HY-14951
Dmp696	Medchemexpress	Cat# HY-1213
Antalarmin HCl	Medchemexpress	Cat# HY-103377
Mifepristone (RU486)	Medchemexpress	Cat# HY-13683
Metyrapone	Medchemexpress	Cat# HY-B1232
Scopolamine	Selleckchem	Cat# S9326
Resifineratoxin	Alomone Labs	Cat #R-400
Kappa bungarotoxin	Alomone Labs	Cat# B-300
recombinant murine G-csf	Peprotech	Cat# 250-05
recombinant Acth	R&D	Cat# 3492
recombinant murine Cxcl12	R&D	Cat# 460-SD
Critical commercial assays		
mouse corticosterone ELISA	abcam	Cat# ab108821
mouse Acth ELISA	abcam	Cat# ab263880
mouse Cxcl12 ELISA	R&D	Cat# MCX120
mouse G-csf ELISA	R&D	Cat# MCS00
mouse Il1b ELISA	R&D	Cat#DY401
mouse Tnfa ELISA	R&D	Cat#DY410
T-PER buffer	Thermo Fisher Sci.	Cat# 78510
BCA assay	Thermo Fisher Sci.	Cat# 23227
TRIzol reagent	Thermo Fisher Sci.	Cat# 15596026
Reliaprep RNA tissue minikit	Promega	Cat# Z6010
RNAsin	Promega	Cat# N2511
M-MLV RT	Promega	Cat# M1701
GoTag qPCR system	Promega	Cat# A6001
CD31 microbeads, mouse	Miltenyi Biotec	Cat# 130-097-418
CD45 microbeads, mouse	Miltenyi Biotec	Cat# 130-052-301
7-AAD	Thermo Fisher Sci.	Cat# A1310
Zombie NIR	Biolegend	Cat# 423105
CountBright absolute counting beads	Thermo Fisher Sci.	Cat# C36950

(*Continued on next page*)

Continued

REAGENT or RESOURCE	SOURCE	IDENTIFIER
Experimental models: Cell lines		
adrenocortical Y1 cells	Bornstein Lab, Technical University of Dresden	N/A
murine Bcr-Abl ALL cells	Pereira Lab, Yale University	N/A
murine bone marrow-derived macrophages	C57BL/6J mice	N/A
L929 cells	DSMZ	#ACC 2
Experimental models: Organisms/strains		
C57BL/6J	Janvier Labs, Yale University and Jackson Laboratories	N/A
B6.129S6-*Nr3c1*$^{tm2.1Ljm}$/J (Nr3c1$^{flox/flox}$)	Jackson Laboratories; via J. Tuckermann	strain #012914
B6.129-*Gt(ROSA)26Sor*$^{tm1(cre/ERT2)Tyj}$/J (Rosa26CreERT2)	Jackson Laboratories	strain #008463
C57BL/6-Tg(Vav1-NUP98/HOXD13)G2Apla/J	Jackson Laboratories	strain #010505
B6.S6JL-Ptrprc^{a} Pepc^{b}/BoyJ (B6 CD45.1)	Jackson Laboratories	strain #002014
B6.129P2(SJL)-*Myd88*$^{tm1.1Defr}$/J	Jackson Laboratories	strain #009088
YRS ST2/IL25/TSLPR TKO	R.Locksley	N/A
Adrb1 tm1Bkk Adrb2 tm1Bkk	Jackson Laboratories	strain #003810
B6(Cg)-*Ifnar1*$^{tm1.2Ees}$/J	Jackson Laboratories	strain #028288
ADX and sham-operated mice	Jackson Laboratories	N/A
Listeria monocytogenes strain: 10403s	R. Medzhitov	N/A
Oligonucleotides		
Actb F: GATCTGGCACCACACCTTCT R: GGGGTGTTGAAGGTCTCAAA	Merck	N/A
Itga4 F: TCTGTGAGTAGGTGGAGGAGATT R: CGGAAGTGACAAATATGCTGCAA	Merck	N/A
Cxcr4 F: TACATCTGTGACCGCCTTTA R: GGCAAAGAAAGCTAGGATGA	Merck	N/A
Cxcl12 F: AGCCAACGTCAAGCATCTGA R: TCGGGTCAATGCACACTTGT	Merck	N/A
Crhr1 F: ACAAACAATGGCTACCGGGA R: AAAGCCGAGATGAGGTTCCA	Merck	N/A
cFos F: GTCCGGTTCCTTCTATGCAG R: TAAGTAGTGCAGCCCGGAGT	Merck	N/A
Mc1r F: TTGGTGCCTGTATGTGTCCA R: CACGATGCTGACACTTACCATC	Merck	N/A
Mc2r F: TGCAGCTGACCGTTACATCA R: AGCATCAAAGGGAACAGCGA	Merck	N/A
Mc3r F: TATCCACATGTTCCTCTTCGCC R: TTGAAATGGGCCGTGTAGCA	Merck	N/A
Mc4r F: TTTTACGCGCTCCAGTACCA R: AATGTGAAGCCTCGCCATCA	Merck	N/A
Mc5r F: AATCTTACCCTGAACGCCTCA R: ACATGGGTGAGTGCAGGTTT	Merck	N/A

(*Continued on next page*)

Continued

REAGENT or RESOURCE	SOURCE	IDENTIFIER
Software and algorithms		
FlowJo v10	FlowJo	www.flowjo.com
Prism V9	Graphpad	www.graphpad.com
BioRender	BioRender	www.biorender.com
ImageJ	NIH	https://imagej.nih.gov/ij/download.html
Single Cell Portal	Broad Institute	https://singlecell.broadinstitute.org/single_cell
Tabula Muris	Tabula Muris Consortium	https://tabula-muris.ds.czbiohub.org
Primerblast	NIH	https://www.ncbi.nlm.nih.gov/tools/primer-blast/
Primer3	N/A	https://primer3.ut.ee

RESOURCE AVAILABILITY

Lead contact

Further information and requests for resources or reagents should be directed to and will be fulfilled by the lead contact, Nikolai P. Jaschke (nikolai.jaschke@yale.edu)

Materials availability

This study did not generate unique new reagents.

Data and code availability

- This paper analyzes existing, publicly available data as listed in the key resources table.
- This paper does not report original code.
- All original data reported in this manuscript will be shared by the lead contact upon reasonable request.

EXPERIMENTAL MODEL AND STUDY PARTICIPANTS DETAILS

Mice

C57BL/6J wildtype mice were obtained from Janvier Laboratories (Le Genest-Saint-Isle, France) at the age of 6-8 weeks or bred in-house at Yale University. Mice from external sources were allowed to acclimatize to local conditions for a minimum of 7-10 days before being subjected to experimental procedures. Animals were housed in groups of up to 5 mice/cage at the animal facility of the Technical University (TU) of Dresden or Yale University and kept under a 12h light:dark cycle with *ad libitum* access to water and food. *Nr3c1*$^{fl/fl}$ mice were kindly provided by Jan Tuckermann (University of Ulm, Germany) and crossed with Rosa26-CreERT2 mice to obtain *Nr3c1*$^{fl/fl;Rosa26\text{-}CreERT2}$ animals. Mice from both sexes were used, which were heterozygous for the Cre allele, whereas Cre-negative littermates served as controls. DNA was isolated from ear clips and genotyping was performed according to standardized protocols. Both genotypes were injected with tamoxifen dissolved in sunflower oil (100µl, 10g/L) at the age of 6-7 weeks and used for *in vivo* experiments 2 weeks later. B6.S6JL-Ptrprc^{a} Pepc^{b}/BoyJ (B6 CD45.1) and C57BL/6-Tg(Vav1-NUP98/HOXD13) G2Apla/J (MDS model) mice were obtained from Jackson Laboratories (Bar Harbor, ME, USA) and bred at TU Dresden. Adrb1/b2 double knock-out (KO), Myd88 KO, and IFNAR1 KO mice were all obtained from the Jackson Laboratory and bred at Yale University. YRS ST2/TSLPR/IL25 TKO were kindly provided by Dr. Richard Locksley (University of San Francisco). Animals were used between the age of 6-12 weeks for experimental procedures. Adrenalectomized (ADX) animals were also purchased commercially. Following surgical removal of the two adrenal glands, animals were closely monitored for 2 weeks at the local facility. Sham operated animals served as controls. All mice received 0.9% saline solution instead of regular drinking water until further experimental procedures, which were conducted 3 weeks post-surgery.

After experimental interventions (see next sections) were terminated, mice were anaesthetized using ketamine/xylazine anesthesia and sacrificed by cervical dislocation. Blood was obtained by cardiac puncture or retroorbital bleeding. Organs were either collected in PBS or formaldehyde for further processing or immediately snap frozen in liquid nitrogen. For small volume blood sampling, the retroorbital plexus was punctured using thin capillaries. Blood was collected in EDTA- or heparin-coated tubes. All mouse experiments were initiated between ZT23 (05:00 AM) and ZT2 (08:00 AM) if not otherwise stated.

Animal experiments were approved by local authorities (TUD, protocol TVV 22/2022 and Yale University's Institutional Animal Care and Use Committee) and performed according to institutional guidelines.

Human study participants

Patients from both sexes were included in our study if the following inclusion criteria were met (1) diagnosis of Rubinstein Taybi syndrome (RSTS) by genetic testing (either pathogenic or likely pathogenic mutation in *CREBBP* or *EP300*) (2) at least one determination of white blood cell count (3) written informed consent for collection, analysis, and publication of relevant data obtained from the patient or legal guardians. Exclusion criteria were: (1) insufficient data available, (2) refusal to participate in the study. The PID-GENMET and FISIOPAT-PID studies were approved by the institutional review boards/ethic committee of Comitato Etico Brianza (Monza, Italy) and conformed to the Declaration of Helsinki. Data was collected between 2007 and 2019. All laboratory results were analyzed with reference to age-matched normal ranges. Leukocytosis was defined as leukocyte counts exceeding the age-matched upper reference limit of normal.[77]

Bone marrow cultures and murine bone marrow derived macrophage (mBMDM) differentiation

Animals were sacrificed to obtain femora and tibias. Bones were crushed in FACS buffer (PBS, 2% FCS and 5 mM EDTA) using a mortar. Residual skeletal tissue was removed and cell suspensions were filtered through 70μm cell strainers to yield single cells. Suspensions were centrifuged at 1800 RPM for 5 min, followed by erythrocyte lysis using ACK buffer (Thermo Fisher Sci, Waltham, MA). After another centrifugation step, the pellet was dissolved in RPMI medium supplemented with 10% FCS, 1% penicillin/streptomycin (P/S), 2mM glutamine and 1x non-essential amino acids (NEAAs) (Gibco, Thermo Fisher Sci, Waltham, MA). Cells were seeded into 6-well plates at a density of $5x10^6$ cells/well and used for *in vitro* studies on the same day. Following treatment, cell cultures were washed, pelleted by centrifugation and snap-frozen in liquid nitrogen for downstream analysis. Each bone marrow culture corresponds to a biologically independent replicate (mouse). For experiments with flow cytometry read-outs, cells were directly seeded into FACS tubes, centrifuged and resuspended in media containing the indicated treatments. Cells were then incubated at 37 or 4°C, followed by downstream processing for flow cytometry as described elsewhere in this section.

To obtain macrophages, bone marrow cultures were exposed to differentiation medium for 7 days consisting of RPMI supplemented with 30% L929 conditioned medium as a source for G-csf, 10%FCS, 1% P/S, 2mM glutamine and 1x NEAAs. After confirmation of successful differentiation by microscopy, cells were subjected to experimental treatments.

Y1 cell culture

Immortalized murine adrenocortical cells (Y1) were kindly provided by the Bornstein Lab (TU Dresden, Germany). Cells were grown in 75mm2 flasks and F-12 K Medium supplemented with 2.5% horse serum, 15% FCS, 1% P%S. Cultures were maintained under a humidified atmosphere at 37°C and 5% CO2. One day before being challenged with different reagents, cells were seeded in 6-well plates at a density of 150 000 cells/well. Treatment conditions are specified in the figure legends.

METHOD DETAILS

Drugs and treatments

All drugs, peptides, antibodies and chemicals administered in this study are summarized in the key resources table. A485 was injected i.p. or i.v. (10 or 5μl/g body weight) at 100 mg/kg as previously reported.[29] For selected experiments, lower or higher doses were chosen as denoted in the respective figures. A485 stock solutions were prepared by dissolving the drug in prewarmed DMSO at 200 mg/ml, followed by steady shaking for 5-10 min. For *in vivo* experiments, the stock solution was diluted in a mix of PEG300 (Sigma Aldrich, St.Louis, MO), Tween80 (Serva, Heidelberg, Germany) and sterile water (30/5/60%, respectively). The resulting liquid was mixed rigorously and ultrasonication was applied if necessary. Aliquots were prepared after all components were successfully dissolved. Controls received an equivalent amount of vehicle solution containing 5% pure DMSO instead of A485 in DMSO. Aliquots were stored at -80°C and used within 4-6 weeks. All other drugs used in this study were likewise dissolved in DMSO/PEG300/Tween80/water or PBS as appropriate. Recombinant proteins were freshly dissolved in sterile PBS immediately before use and injected i.v. (100μl/mouse) under short isoflurane anesthesia. The following drug doses were used: 20 mg/kg C646, 20 mg/kg SGC-CBP30, 150 mg/kg 5-FU, 0.2 mg/kg fingolimod, 5 mg/kg NU9056 (Tip60 inhibitor), 5 mg/kg AMD3100, 50 mg/kg firategrast, 25 mg/kg dmp696, 20 mg/kg antalarmin, 20 mg/kg mifepristone (RU486), 50 mg/kg metyrapone, 1 mg/kg scopolamine, 1 mg/kg kappa bungarotoxin, 250 μg/kg rG-csf, 10μg rActh/mouse, 20μg anti-G-csf or isotype control (IgG)/mouse, 8 mg/kg anti-IL6R or rat IgG isotype control. Metyrapone and rActh were administered twice (90 and 45 min between injections, respectively) during the corresponding experiments due to their short half-lives. Neutralizing antibodies and isotype controls were applied 16-18h prior to the experimental challenge. The RTX model is described elsewhere in this section. Loss of function of peripheral sympathetic nervous system neurons was induced by i.p. injection of 6-OHDA (100mg/kg) twice (d1 and d3) into 8 to 10-week-old wildtype mice. Experiments were conducted two days after the second injection (d5).

Listeria monocytogenes infection and quantification of bacterial burden

Toxic bone marrow injury was induced by a single i.p. injection of 5-FU (150 mg/kg). Controls received an equivalent volume of PBS. *Listeria monocytogenes* (*L. monocytogenes*) strain 10403s was originally obtained from the laboratory of Dr. Daniel Portnoy and kindly provided by Dr. Ruslan Medzhitov. *L. monocytogenes* was grown to log-phase in brain heart infusion (BHI) broth, washed once with PBS, and stored as stock solutions at -80°C ($2x10^{10}$ CFUs/ml). For infection of mice, stock solutions were diluted in PBS and mice were injected retro-orbitally with $7.5x10^4$ CFUs of *L. monocytogenes* (in 100μl PBS). Mice were infected on the sixth

day after 5FU exposure around ZT21 (4:30 AM), followed by i.p. treatment with A485 (100 mg/kg) or an equivalent volume of vehicle solution 1h later (5:30 AM). For *L. monocytogenes* infection in immunocompetent hosts (PBS- instead of 5FU-injected), a higher dose ($1x10^5$ CFUs) was used, but no mortality was noted. Survival was monitored twice daily for a minimum of 9 (immunocompetent mice) or 21 (immunocompromised mice) days. Immunocompetent mice were sacrificed on day 9 of the experiment without any signs of sickness.

Quantification of bacterial burden was achieved by pushing 50-100 mg of liver or spleen tissue though 70μm cell strainers using the plunger of a 5ml syringe, followed by flushing with plain RPMI medium. The resulting homogenates were mixed with 1% TritonX100 (diluted in H2O) and subjected to serial dilutions, which were plated on BHI agar plates (Hardy Diagnostics) using sterile plastic loops. Bacteria were allowed to grow at 37°C for 24 hours. CFU's were counted manually and results were expressed as number of CFUs/g of tissue.

Intravascular leukocyte labeling

Labeling of the intravascular leukocyte compartment was achieved by retroorbital injection of 2μg of fluorophore labeled CD45 antibodies (CD45 APC) dissolved in 100μl PBS 2–3 min before sacrifice, followed by immediate organ collection. Blood and tissues were subjected to preparation for flow cytometry as described elsewhere in this section. Intravascular leukocytes were defined as ''double CD45 positive'', if they were labeled with both the intravascularly applied CD45 antibody as well as the second CD45 antibody (CD45 PE-Cy7), which was added to cell preparations during flow cytometry staining. ''Single CD45 positive'' cells stained positive for CD45 PE-Cy7 only (extravascular).

Cell tracking

In vivo tracking of CD45+ cells was achieved as previously described.[13] The bone marrow of B6-.S6JL-Ptrprc^a Pepc^b/BoyJ (referred to as B6 CD45.1) mice was obtained as described elsewhere in this section; 10-20$x10^6$ bone marrow cells (diluted in 200 μl PBS) were adoptively transferred into C57BL/6J wildtype mice through retroorbital injection at ZT16. After 8 to 9h (ZT0/1), mice were either sacrificed for confirmation of successful bone marrow homing or treated with A485 or vehicle for 5h, followed by organ collection and flow cytometry analysis.

Conventional and automated flow cytometry analysis

Blood was collected in EDTA-coated tubes and erythrocyte lysis was performed using ACK lysis buffer (Thermo Fisher Sci., Waltham, MA). Tissues (lung, liver, muscle) were collected in PBS, weighed and minced in a mixture of DMEM supplemented with collagenase (1.2 mg/mL) and dispase II (25 U/mL) (both from Sigma-Aldrich, St.Louis. MO), followed by digestion at 37°C under steady shaking at 800 rpm for 45 minutes. Homogenates were then flushed through 40 or 100μm cell strainers (Sigma Aldrich, St.Louis, MO) to yield single cell suspensions. Spleens were immediately pressed through cell strainers without prior digestion. Bone marrow homogenates were obtained by crushing tibias and femora in FACS buffer (PBS, 2% FCS and 5 mM EDTA) using a mortar. Residual skeletal tissue was removed and homogenates were passed through 40μm cell strainers. For both the spleen and bone marrow, erythrocyte lysis was performed as described above. Single cell suspensions were stained in FACS buffer containing fluorophore-conjugated antibodies at a concentration of 1:400 at 4 degrees for 30 min. Prior to adding primary antibodies, unspecific bindings sites were blocked using anti-CD16/32 antibodies. Live and dead cells were differentiated by DAPI or 7-AAD staining (both diluted 1:1000) as shown in the respective gating examples. For quantification of progenitor populations in the bone marrow, single cell suspensions were stained by DAPI (0.1μg/ml) and DAPI-negative cells were counted by MACSQuant Analyzer (Miltenyi Biotec, Cologne, Germany), followed by stained with a c-Kit bio antibody. Anti-Biotin MicroBeads were added to enrich for c-Kit$^+$ cells using LS columns.

Cells were identified as: 1.) HSCs: Lin$^-$ (negative for B220, CD3ε, CD19, NK1.1, Gr1, Ter119, and CD11b) Sca1$^+$ c-Kit$^+$ (LSK) CD48$^-$ CD150$^+$, 2.) MPP2: LSK CD48$^+$ CD150$^+$, 3.) MPP3/4: LSK CD48$^+$ CD150, 3.) MPP3/4: LSK CD48$^+$ CD150$^-$, 4.) CMP: LK CD16/32$^-$ CD41$^-$ CD105$^-$ CD150$^-$, 5.) Leukocytes: single CD45+, 6.) Neutrophils: CD45+,Cd11b+,Gr1+, 7.) B lymphocytes: CD45+, Cd11b-, CD3-, CD19+, 8.) T lymphocytes: CD45+, Cd11b-, Cd3+, CD19-.

Antibodies used in this study are summarized in the key resources table. All flow cytometry experiments were performed using counting beads (Countbright, Thermo Fisher Sci., Waltham MA) if not otherwise stated. Data were acquired on a BD LSR Fortessa (BD Biosciences), BD LSR II, BD FACSAria II, BD LSRFortessa X-20, or a BD FACSCanto II (all from BD Bioscience) and analyzed using FlowJo v10 software (Tree Star Inc.). The abundance of cells within tissues was normalized according to the respective weight and expressed as number of cells per mg of tissue. Exemplary gating strategies are shown in Figures S10–S13.

Automated fluorescence-flow cytometry analysis was performed using XN-1000 (Sysmex) or Hemavet 950 (Drew Scientific) devices, allowing for complete blood count and white blood count differential measurements. Murine blood (2-3 drops) was collected in EDTA- or heparin-coated tubes, followed by analysis on the same or subsequent day.

Hypothalamic explants

Following sacrifice, brains were extracted from WT mice and hypothalami were explanted as previously described[10] under sterile conditions. Whole tissue explants were cultivated in DMEM F-12 (Gibco, Thermo Fisher Sci, Waltham, MA) supplemented with 10% FCS, 2 mM glutamine, 1x non-essential amino acids and 1% pencilline/streptomycine. A485 (5μM) or vehicle (DMSO) were immediately added, and tissue was harvested 3h later for downstream processing.

A485 measurements

A rapid and sensitive liquid chromatography tandem mass spectrometry (LC-MS/MS) method was developed and validated for the determination of A485 in serum and tissue. Frozen serum samples (-20 °C) were thawed at room temperature, mixed and centrifuged. Volumes of 50 μl serum were diluted with 100 μl acetonitrile and mixed and centrifuged for 10 minutes (14.000 U/min). Volumes of 50 μl cell lysates were diluted with 100 μl solvent AB (a mixture of acetonitrile, 2 mM ammonium acetate solution and formic acid; 50/50/0.05, v/v/v); 20 μl of the clear supernatant was injected into the API 4000 LC-MS/MS system. Measurements were performed using an Ultimate 3000 HPLC system from Thermo Scientific (Waltham, MA, USA) The flow rate was 0.5 ml/min. A485 was determined using a Synergi 4μ Fusion-RP 80A, 150 x 2.0 mm column (Phenomenex, Torrance, CA, USA) with a mobile phase gradient. The flow rate was 0.5 ml/min. The retention time of A485 was 3.77 min. The HPLC system was coupled to an API 4000 tandem mass spectrometer (AB Sciex, Framingham, MA, USA) with an electrospray interface. The detection was performed in multiple reaction monitoring (MRM) mode, using the three most intensive transitions. The product ion transition with the highest intensity was used for quantification (quantifier) and the other transitions were used for confirmation (qualifier).

Mass spectrometric conditions

Substance	Precursor ion	Product ion	Cone voltage (V)	Collision energy (eV)
A485_1	537.3	493.3	101	15
A485_2	537.3	272.3	101	23
A485_3	537.3	215.2	101	39

In preliminary tests, we found that the expected concentration range was large. Accordingly, the upper standard was set at 1,000 ng/mL. Two-fold serial dilutions were performed to yield a standard curve with the lowest standard set at 3.91 ng/mL. Finally, the standard samples were completed with a blank serum. Samples above the calibration range were diluted 1:10 or 1:100 with solvent AB and measured again.

Ablation of TRPV1+ sensory neurons

Mice received increasing doses (30, 70 and 100μg/kg) of resiniferatoxin (referred to as "RTX", Alomone Labs, Israel) on three consecutive days via subcutaneous injections at the age of 4 weeks as previously described.[78] The RTX stock solution was dissolved in DMSO and diluted in PBS to the desired concentration. Controls received an equivalent volume of DMSO/PBS solution. Successful targeting of TRPV1 sensory neurons was confirmed by progressive greying of fur[79] and loss of heat sensitivity. Mice were subjected to further experimental procedures 4 weeks after the last injection.

Acetyl CoA quantification

Murine bone marrow derived macrophages were differentiated from bone marrow precursors as described elsewhere in this section. Following treatment with DMSO or A485, cells were harvested at different time points as indicated in the respective figure, washed, centrifuged to yield a cell pellet and immediately snap-frozen in liquid nitrogen. The pellet was dissolved in 200 μl 30% methanol in Acetonitrile with 0.1 mM ammonium acetate, and 0.01% NH_4OH. As an internal standard, 5 μM Acetyl-1,2-13C2-Coenzym A lithium salt (Sigma Aldrich, St.Louis, MO) was used. After adding 1/3 volume of 0.5 mm metal beads, samples were homogenized for 10 min at 4 °C and 300g in a TissueLyser II (Qiagen, Hilden, Germany). Next, 20 μL of homogenate solution was isolated for protein quantification by the BCA Protein Quantification Kit (Thermo Sci., Waltham, MA). The resulting mixture was centrifuged at 13,000g for 30 min and the supernatant was transferred to a new tube, followed by LC-MS/MS. Chloropropamide (100nM) was used as an additional internal standard. Results were normalized according to the internal standard and total protein content of the respective sample.

The LC–MS/MS analysis was performed on high performance liquid chromatography (HPLC) system (*1200 Agilent*) coupled online to G2-S QTof (*Waters*). For normal phase chromatography, the Bridge Amide 3.5ul (2.1x100mm) column from Waters was used. For the normal phase, the mobile phase composed of eluent A (95% acetonitrile, 0.1 mM ammonium acetate, and 0.01% NH_4OH) and eluent B (40% acetonitrile, 0.1 mM ammonium acetate, and 0.01% NH_4OH) was applied with the following gradient program: Eluent B, from 0% to 100% within 18 min; 100% from 18 to 21 min; 0% from 21 to 26 min. The flow rate was set at 0.3 ml/min. The spray voltage was set at 3.0 kV and the source temperature was set at 120 °C. Nitrogen was used as both cone gas (50 L/h) and desolvation gas (800 L/h), and argon as the collision gas. MS^E mode was used in negative ionization polarity. Mass chromatograms and mass spectral data were acquired and processed by MassLynx software (Waters).

CXCL12 migration assay

Murine Bcr-Abl lymphoma cells (kindly provided by Joao Pereira, Yale University) were grown in petri dishes in DMEM supplemented with 20% FCS, 1% penicillin/streptomycin, HEPES and 2-Mercaptoethanol. Cells were collected, centrifuged and pellets were dissolved in migration buffer (DMEM with 0.5% fatty acid free BSA, HEPES and penicillin/streptomycin). Cells were then transferred into FACS tubes and incubated at 37°C for 30 min before being subjected to experimental procedures. Next, 50 000 cells (in 100μl migration buffer) were added to migration chambers (Corning, NY), in which the bottom chamber contained A485 (1μM), vehicle (DMSO),

recombinant Cxcl12 (100 ng/ml) or medium without any supplements as indicated in the corresponding figure. Cells were allowed to migrate for 3h at 37°C before being collected from the bottom chamber. Quantification of migrated cells was achieved by flow cytometry following live/dead staining with DAPI.

Magnetic-assisted cell sorting (MACS)

CD45- and CD31-positive cells were sorted from the blood and bone marrow using microbeads (Miltenyi Biotec, Cologne, Germany) and magnetic columns according to the manufacturer's protocol by positive selection. Following preparation of single cell suspensions, cells were counted, centrifuged and the supernatant was removed, followed by resuspension in MACS buffer and addition of microbeads, both of which were adjusted according to the total number of cells. Suspensions were then incubated at 4 °C for 15-30 min, followed by addition of the staining antibody, washing steps and centrifugation. Cells were resuspended in MACS buffer and separated using magnetic columns. The flow-through was collected and labelled as "negative", whereas the bound fraction corresponded to "positive" cells (i.e. cell population of interest). Both fractions were subjected to downstream analysis. Successful enrichment of the population of interest was confirmed by qPCR analysis.

Quantitative polymerase chain reaction (qPCR)

RNA isolation was performed using TRIzol reagent (Thermo Fisher Sci., Waltham MA) or the Reliaprep kit (Promega, Fitchburg, MA) according to the manufacturer's instructions. RNA pellets were diluted in RNAse-free water and its quality was assessed by Nanodrop2000 (Thermo Fisher Sci., Waltham, MA); 250-500 ng of RNA were subjected to cDNA synthesis using random primers (Thermo Fisher Scientific, Waltham, MA), dNTPs (Carl Roth GmbH, Karlsruhe, Germany), M-MLV RT, and RNAsin (both from Promega Corp., Fitchburg, WI). Quantitative polymerase chain reaction was performed using GoTaq Mastermix (Promega Corp., Fitchburg, WI) and forward and reverse primer pairs (sequences are listed in the key resources table). Primer sets were validated by melting curve analysis. All qPCRs were run on a StepOnePlusTM cycler (Applied Biosystems, Carlsbad, CA). Relative mRNA expression of selected targets was calculated using the ΔCT or ΔΔCT method as appropriate. Beta actin (*Actb*) served as the housekeeping gene for normalization.

Protein isolation and immunoblotting

Proteins were isolated from cells and tissues using RIPA or T-PER buffer (Thermo Fisher Sci, Waltham, MA), supplemented with protease and phosphatase inhibitor cocktail (Thermo Fisher Sci, Waltham, MA). To obtain lysates, T-PER was added to tissue according to its weight, followed by homogenization using metal beads. Lysates were rested on ice for 10 min before undergoing centrifugation (10 000g, 5 min, 4°C). Total protein concentration in supernatants was assessed by BCA assay (Thermo Fisher Sci, Waltham, MA) and lysates were subjected to downstream analysis.

Immunoblotting was performed as previously described[65] using SDS page gel electrophoresis, followed by transfer of separated proteins onto 0.2 μm nitrocellulose membranes, which were blocked with 5% BSA. Primary antibodies were applied at 1:500-1:1000 dilution and incubated at 4°C overnight under steady shaking. Signals were visualized using HRP conjugated secondary antibodies and ECL substrate (Thermo Fisher Sci, Waltham, MA). All antibodies used are listed elsewhere in this section.

Enzyme-linked sorbent assays (ELISAs)

Serum was collected from whole blood following centrifugation at 5000 RPM and 4°C for 15 min and used for further assays. The following commercially available ELISAs were used: corticosterone and Acth ELISA (both from abcam, Camebridge, MA), Cxcl12-, interleukin 1 beta-, tumor necrosis factor alpha- and G-CSF-ELISA (all from R&D, Minneapolis, MN). Dilutions were chosen depending on the experimental conditions (undiluted to 1:250). Cxcl12 levels in bone marrow lysates were normalized according to total protein content of the respective samples. For the Acth ELISA, blood was immediately cooled on ice, centrifuged and subjected to the downstream assay within 1h.

Sublethal Irradiation

For sublethal irradiation, mice were exposed to 4 gray and successful induction of bone marrow injury was confirmed by flow cytometry 3 days later.

Immunofluorescence analysis

Following sacrifice, mice were perfused with PBS and 4% PFA for immediate fixation of organs. Brains were extracted and placed in 4% PFA for 8 h, followed by 3 x 10-min washes in 1xPBS. Tissues were then placed in 30% sucrose (diluted in 0.1 M phosphate buffer) at 4°C for 48h. After another wash, brains were embedded in OCT and stored at -80°C until further processing. Sectioning of brains in 40μm slices was achieved using a cryostat. Free-floating sections were washed in PBS-T (0.1% Tween 20 in PBS) 3x for 10 min each under steady shaking at room temperature (RT). Sections were blocked with 10% BSA in PBS-T for 2h under steady shaking at RT, followed by incubation with anti-cFos antibodies (Sigma-Aldrich, 1:2000 diluted in PBS-T) at 4°C for 48h. Free-floating sections were washed again with PBS-T (3 x 10 min, under steady shaking at RT) and finally incubated with an Alexa Fluor 594-conjugated goat anti-rabbit IgG (1:1000) at RT for 2 h. After 3 x 10 min washes with PBS-T, sections were mounted using Fluoroshield™ with DAPI (Sigma-Aldrich, F6057) and coverslipped. Fluorescence imaging was performed on a Nikon ECLIPSE Ti2 inverted microscope (Nikon Instruments Inc.) using a triple bandpass filter cube (TRITC, FITC, DAPI) from Nikon, with a Cool LED

pE-300 and excitation wavelengths at 370nm for DAPI and 550nm for Alexa Fluor 594. Images were obtained with an Andor Sona Camera with a 20x objective and consistent settings including exposure time (DAPI: 300ms, Texas Red: 500ms). The images were further processed on the software Fiji (is just ImageJ®), where the set display rate was kept consistent across images for comparison.

LDH release assay

Cell toxicity was estimated by measuring LDH activity in cell culture supernatants over time using the LDH-Glo assay (Promega, Fitchburg, MA) according to the manufacturer's instructions.

Organ toxicity screen

Markers of organ damage including alanine and aspartate aminotransferase (ALT and AST, respectively), blood urea nitrogen (BUN), creatinine kinase (CK) and troponin T (TnT) were determined in serum samples 24h post A485 injection by routine measurements at the Department of Clinical Chemistry of the Technical University of Dresden.

QUANTIFICATION AND STATISTICAL ANALYSIS

Experimental data is shown as mean ± s.e.m. if not otherwise stated. Each dataset comprises a minimum of 3 biologically independent replicates. Key experiments were repeated at least twice and confirmed by independent scientists where applicable. Sample size calculations were based on expected effect sizes and previously published literature. Baseline measures of selected variables in kinetic experiments with genetically identical organisms were obtained from 3-6 randomly selected animals. Comparisons between groups of two were assessed by student's unpaired t-test for parametric and Mann Whitney U test for non-parametric data. Groups of three or more were compared by ordinary one-way ANOVA with Holm Sidak's post hoc test adjusted for multiple comparisons or Fisher's LSD as stated in the figure legends. Groups stratified according to two independent variables (e.g. genotype and treatment) were compared by two-way ANOVA with Holm-Sidak's post-hoc test. Frequencies of categorical variables were analyzed by chi square (χ^2) test. Probability of survival was assessed by Mantel Cox Test. All statistical tests were two-tailed. Where applicable, datasets were screened for outliers using Grubb's test, which allowed for exclusion of a single data point per group and dataset (alpha=0.05). Statistical significance was assumed at P-values <0.05. Data analysis and visualizations were performed using Prism V9 (Graphpad Inc, LaJolla, CA).